



# Nomenclature

## Acronyms / Abbreviations

1-D	One-Dimensional
AFM	Atomic Force Microscopy
AlN	Aluminium Nitride
BSE	Back Scattered Electron
BSF	Basal-plane Stacking Fault
C-AFM	Conductive Atomic Force Microscopy
EBL	Electron Blocking Layer
EL	Electroluminescence
ET	Electron Tomography
FIBT	Focussed Ion Beam Tomography
FSR	Free Spectral Range
GaAs	Gallium Arsenide
GaN	Gallium Nitride
InN	Indium Nitride
LED	Light-Emitting Diode
PD	Partial Dislocation
PSF	Prismatic Stacking Fault

SEM	Scanning Electron Microscope
SE	Secondary Electron
SPS	Single Photon Source
WGM	Whispering Gallery Mode



# Chapter 3

## Inhomogeneous Electroluminescence in InGaN QW LEDs

### 3.1 Background

$\text{In}_x\text{Ga}_{1-x}\text{N}/\text{GaN}$  QW structures are key structures in present day light emitting diodes in the visible wavelengths. Despite the growth of III-nitride LEDs into a gigantic market with a projected overall worth of 64 billion EUR by 2020, III-nitride alloys suffer from a plethora of material issues arising from heteroepitaxial growth on foreign substrates with large lattice mismatches [6] such as the formation of defects, as mentioned in section 1.1.4. As discussed in section 1.1.4, whilst III-nitride optoelectronic devices appear relatively robust to dislocations relative to other III-V devices, threading dislocations can nonetheless be source of highly undesirable effects in diode structures.

Threading dislocations have been shown to result in inverted pyramidal defects at the surface of nitride epilayers, known as 'V defects'. The effect of these defects on LED performance is hotly debated in literature as they are expected by many to hinder LED performance, as previously discussed in section 1.1.4.4. However, it has been shown that narrower QWs along the sidewalls of V-defects serve to screen carriers from non-radiative centres at TDs [34].

In this study, a 'multi-microscopy' approach, whereby several microscopy techniques are utilised on the same features, is used to elucidate the origin of inhomogeneous EL in  $\text{In}_x\text{Ga}_{1-x}\text{N}/\text{GaN}$  QW structures. The correlation of emissive and structural properties at the surface of the LED structures using several microscopy techniques has allowed for the detection of hexagonal defects at the centre of the inhomogeneities. Following this, structural and compositional information obtained using a combination of techniques is used to simulate

and reproduce the inhomogeneous EL, thus elucidating the mechanism whereby hexagonal defects can cause inhomogeneous EL in LEDs.

### 3.2 Sample Structure

For this study, a QW InGaN LED structure with a nominal QW thicknesses of 4.5 nm was studied. The sample was grown at the Cambridge Centre for Gallium Nitride, with LED processing carried out at the University of Bath. The structure was grown on a low dislocation density ( $5 \times 10^8 \text{ cm}^{-2}$ ) GaN template on sapphire, and consists of a 2  $\mu\text{m}$  layer of unintentionally doped GaN followed by a 3  $\mu\text{m}$  silicon doped GaN layer. The active layer consists of a 5 period InGaN/GaN MQW region, with unintentionally doped GaN barriers (7.6 nm). An AlGaN electron blocking layer (20 nm) and a magnesium-doped GaN cap (117 nm) were grown following the active region. The sample code is C5608A. This is shown schematically in Fig. 3.1:



Fig. 3.1 LED structure schematic.

The wafer was processed into  $1 \times 1 \text{ mm}^2$  side contacted LEDs with thin oxidized Ni/Au current spreading *p*-layer Ohmic contact. Ti/Al Ohmic contact stripes were deposited on the *n*-layer and the Ni/Au current spreading layer in an interdigitated geometry.

QW thickness for the sample was determined from X-ray diffraction (XRD) using the method described by Vickers *et al.* [9]. The QWs were grown using the '2T' method, whereby the growth temperature is ramped up immediately following the InGaN growth under ammonia but without metalorganic fluxes. The barrier growth begins towards the end of the temperature ramp, this typically leads to loss of indium during the temperature ramp which can cause gross well-width fluctuations [101] but a higher barrier growth temperature is preferable[102]. '2T' growth is shown schematically in Fig.3.2.

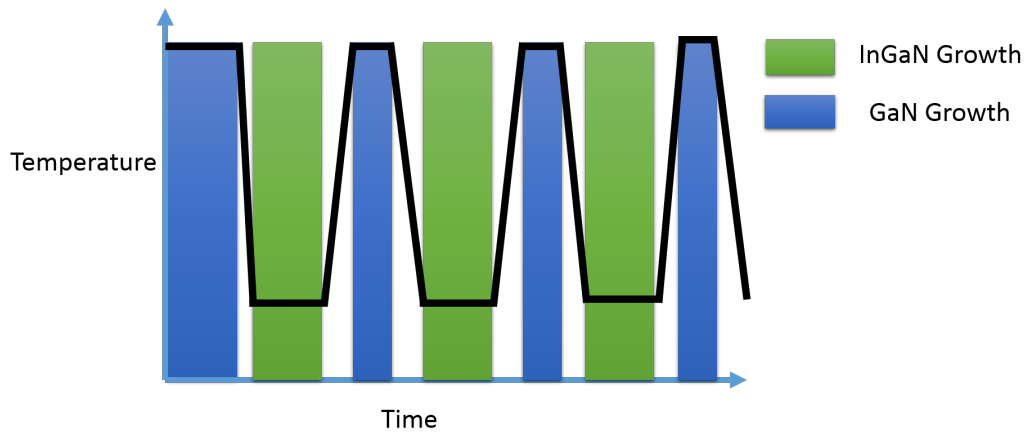


Fig. 3.2 '2T' growth of InGaN/GaN QWs. GaN QB growth is halted during the temperature ramp. The black trace indicates growth temperature over time.

### 3.3 Experimental

Initial evaluation of the inhomogeneous EL was performed in a Signatone S-1160 probe station under forward bias, as shown in Fig.3.3.

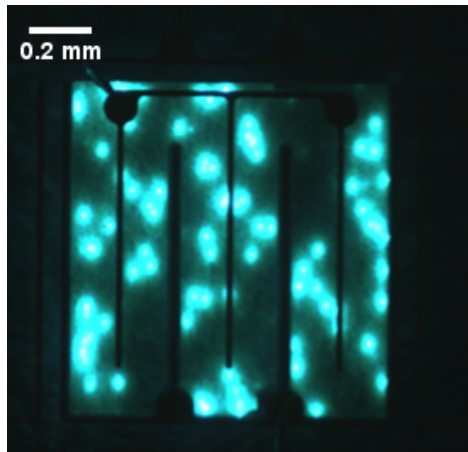


Fig. 3.3 LED EL under a forward bias of 3V. The bright inhomogeneities are visible in the emission of the LEDs.

Following this, hyperspectral EL mapping with CL and EBIC were performed using a modified Cameca SX100 electron probe micro-analyser with a custom built cathodoluminescence set-up. Hyperspectral EL measurements were performed under forward bias, enabling the acquisition spatially resolved EL maps of the inhomogeneities. Following the detection of hexagonal defects at the centre of inhomogeneities using SEM-CL, the defects were analyzed using AFM and C-AFM. Finally, FIB/SEM lamella preparation techniques were used to perform HAADF-STEM and STEM-EDX on the defects, allowing for access nanoscale compositional and structural information required to reproduce the EL in simulations.

### 3.3.1 Hyperspectral EL Imaging

Hyperspectral EL imaging was performed at Strathclyde University with the assistance of Dr Michael Wallace. In order to study the device under forward current, the LED wafers were mounted on TO-5 headers and bonded with 5  $\mu\text{m}$  Al wire. A Keithley Instrument 2401 source meter was used to apply varying forward currents to the devices and thus allow for the collection of EL.

Full EL spectra were collected with a spatial resolution of approximately 3  $\mu\text{m}$  and analysed using custom software developed by Dr. Paul Edwards, allowing for 2-D maps of EL peak intensity, position and FWHM. At each pixel in the map, a full EL spectrum was collected by an Andor CCD spectrograph. A full set of data extracted from the hyperspectral EL mapping (taken from the background emission of the LED, and not the bright inhomogeneities) is shown in Fig.3.4

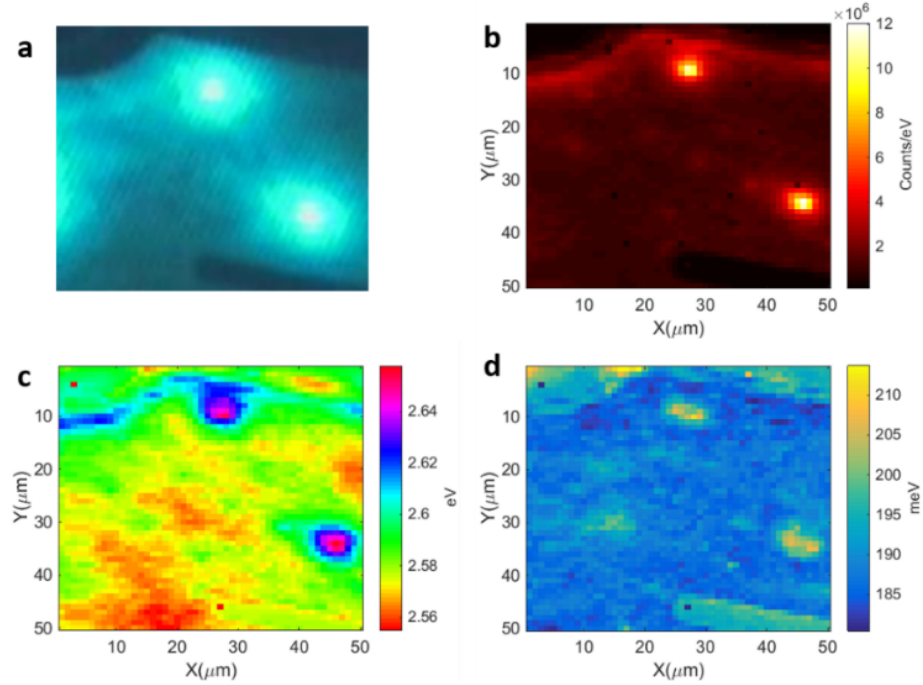


Fig. 3.4 a) Probe station image b) EL peak intensity, c) EL peak energy and d) EL FWHM extracted by fitting the hyperspectral EL data under a forward current of 10 mA

It is interesting to note that from this representative data set, the inhomogeneities observed are brighter by a factor of  $\sim 6$ , blue-shifted in terms of peak energy by  $\sim 0.08$  eV and have a larger FWHM. Although these values were observed to shift based on injection current, the overall trend observed in the EL data collected for this LED is represented by Fig.3.4. All intensity measurements performed on the system at Strathclyde University (for both CL and EL) are reported with units of 'Counts/eV' due to non-uniformity between neighbouring CCD channels in the spectrograph.

### 3.3.1.1 Current Dependent EL Measurements

Current dependent hyperspectral EL maps of the same area were performed, in order to examine the behaviour of the inhomogeneities with increasing current relative to the 'uniform' background. The peak intensities and peak energies for injection currents for device C5608A ranging from 1-250 mA are shown in Figures 3.5 and 3.6 respectively.

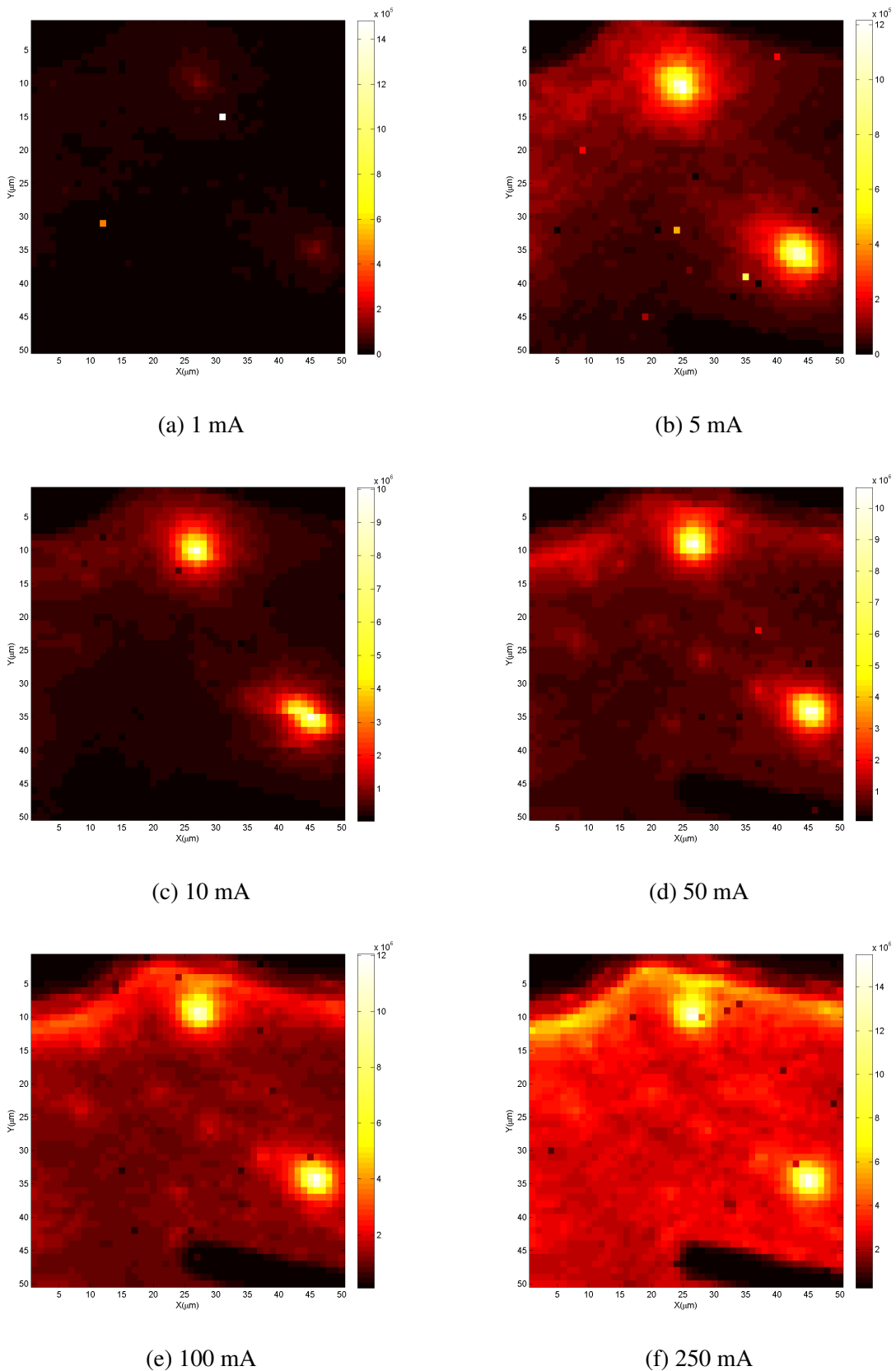


Fig. 3.5 Peak intensity for varying injection current for C5608.

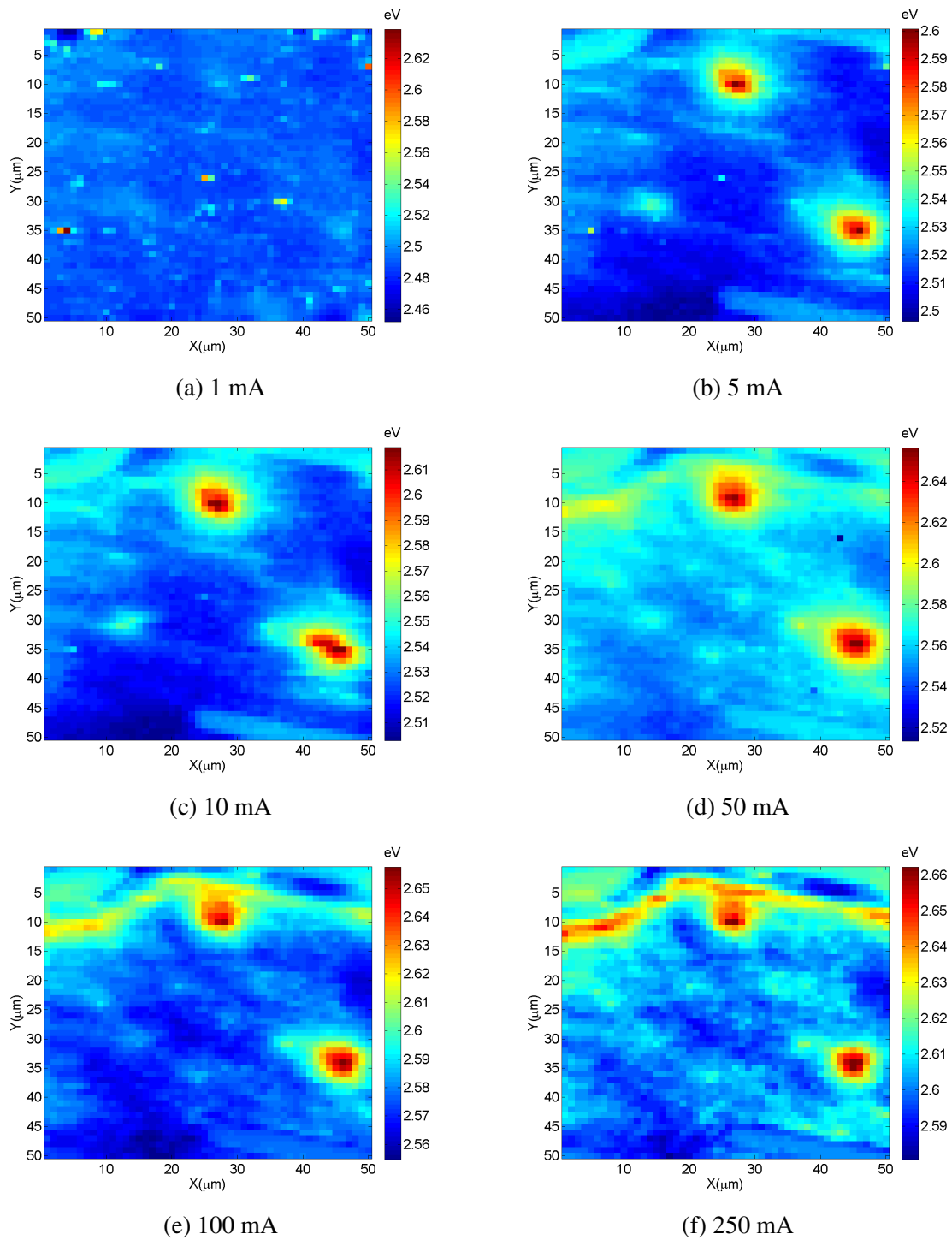


Fig. 3.6 Peak energy for varying injection current for C5608.

The spatially resolved EL data shown in Figures 3.5 and 3.6 allow for the comparison between areas containing the inhomogeneities and the 'background' EL. This is demonstrated in Fig. 3.7 which shows the behaviour of both the inhomogeneities (labelled 'spots') and the averaged background peak intensity with increasing injection current.

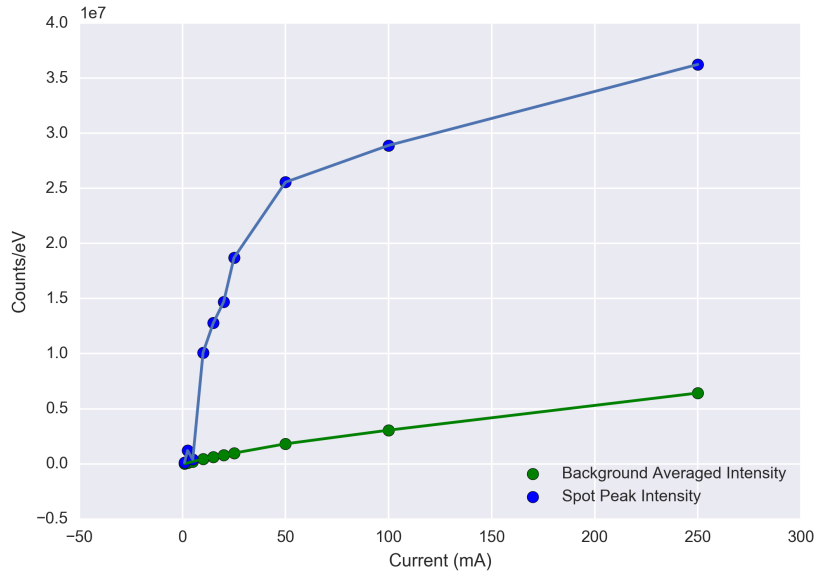


Fig. 3.7 Spot and background average peak intensity against injection current

It is interesting to note that Fig. 3.7 shows the inhomogeneities experience a far sharper initial increase in peak intensity relative to the background based on the hyperspectral EL data fitting in the current range 0-50 mA, perhaps indicating enhanced current injection in the areas exhibiting the inhomogeneities.

Fig. 3.8 shows the same current dependent comparison for background and inhomogeneity peak energy. Here we see the same trend, in that the inhomogeneity exhibits a larger current-induced blueshift in the 0-50 mA range relative to the background. The origin of the current-dependent blueshift in InGaN QW structures is attributed to the screening of the QCSE by the additional carriers injected into the wells [22], and as such indicates the inhomogeneities are regions experiencing higher current injection relative to the background.

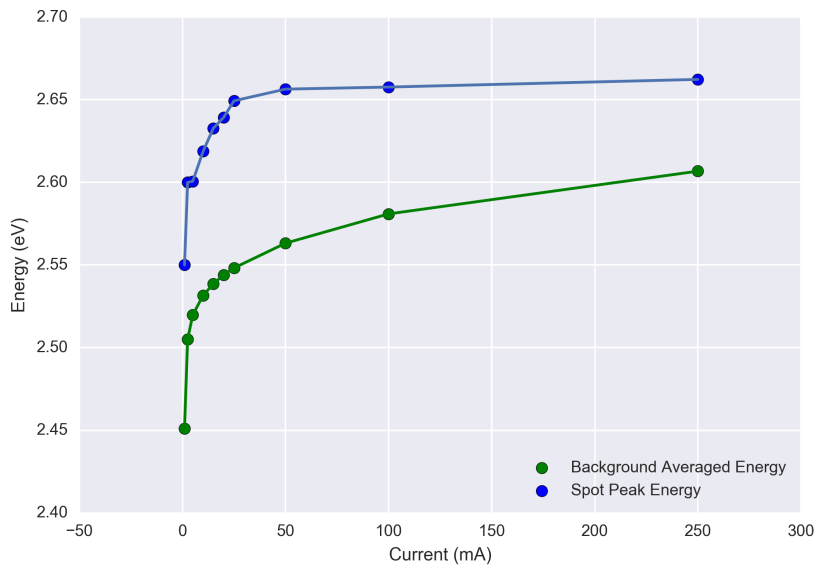


Fig. 3.8 Spot and background average peak energy against injection current

### 3.3.2 Cathodoluminescence and Electron Beam Induced Current

Having noted the behaviour of the inhomogeneities inferred from the hyperspectral EL data, CL and EBIC data were taken over areas containing the inhomogeneities in order to examine their properties in more detail as electron-beam based techniques allow for a far higher resolution than EL mapping.

In order to achieve simultaneous CL and EBIC measurements, a Keithley Instrument 2401 source/measure unit was utilised in order to bias the LED devices at a fixed bias of 0V thus allowing for the measurement of the short circuit current. During the CL image scanning, the Andor CCD camera was set-up to trigger the unit to record the current at each point in the CL spectral acquisition. The CL acquisition was performed with an electron beam at 10 kV and 1 nA. Unfortunately the secondary electron detector was inoperable during the acquisition of this data, as such there is no accompanying SEM micrograph for the CL and EBIC data. The CL and EBIC data for C5608A are shown in Fig.3.9.

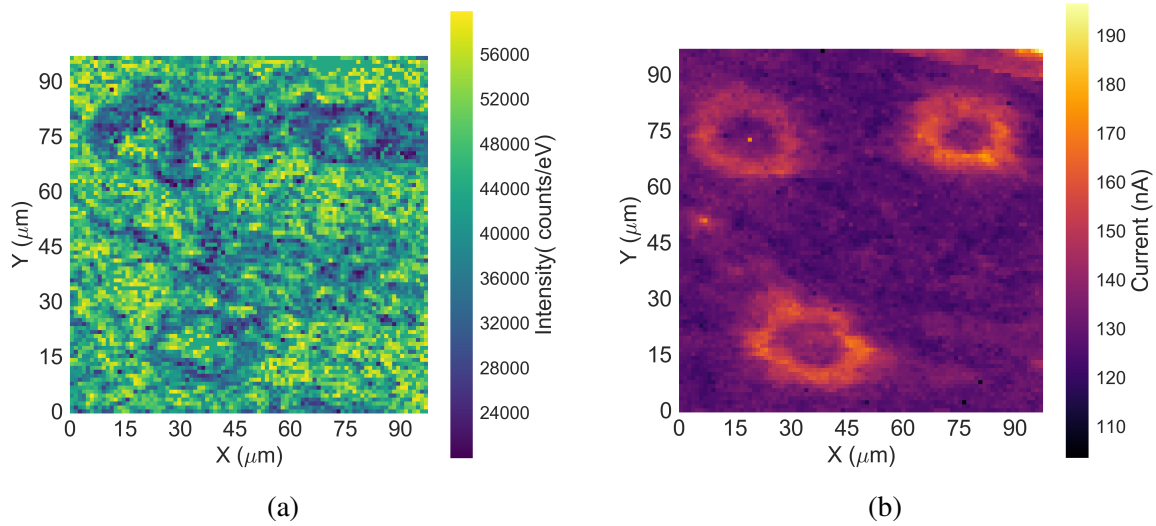


Fig. 3.9 a) CL and b) EBIC maps acquired simultaneously of the area shown in Fig.??b.

Fig.3.9a. shows the inhomogeneities exhibit a lower CL intensity relative to the background, in contrast to the EL. Interestingly, the EBIC signal, shown in Fig.3.9 for both inhomogeneities examined seem rather different. The feature closest to the contact region can be seen as a region of high EBIC surrounding a region of lower extracted current. The low CL intensity detected can be interpreted in several ways: a high density of TDs or point defects could result in non-radiative recombination in these areas [103, 6] or enhanced stress in these regions could result in an enhancement of the QCSE which in turn would redshift and reduce the intensity of the CL emission [15, 22]. The enhanced EBIC in these regions tends to suggest the latter is more likely: the strain enhanced piezoelectric field across the QW stack would likely separate generated carrier-pairs [104] and result in a higher EBIC relative to the less-strained background. We note the size disparity between the features seen here in both the CL and EBIC, which are in the range of 12-15  $\mu\text{m}$  and the inhomogeneities in the EL shown in section 3.3.1.1, which are closer to 10  $\mu\text{m}$  in size. This may suggest that the bright features seen in the EL are in fact contained within the rings shown here, indicating that the features seen here ( reduced CL intensity, enhanced EBIC) may be the outer-boundaries of the features. Further analysis in terms of the CL peak energy as well as structural and compositional information are required to explain the change in CL and EBIC seen here. Unfortunately, the CL spectra were corrupted during data transfer, meaning the information regarding the peak CL energy was lost.

### 3.3.2.1 Scanning Electron Microscopy with Cathodoluminescence

Following the CL and EBIC scans shown in Fig.3.9 performed at Strathclyde University, more detailed SEM-CL experiments were performed at the University of Cambridge using a Philips XL30s field emission SEM at 5 kV equipped with a Gatan MonoCL4 system to record the CL signal. This set-up provides the additional benefit of panchromatic CL imaging, which allows for the detection of the features without the need for detailed EL correlation. Fig. 3.10 shows the morphology of the features in the panchromatic CL and the associated SEM micrograph. The inhomogeneity appears as a region of lower CL intensity, though it is important to note the signal in panchromatic CL mode is the sum of the complete spectrum of photons collected. Nonetheless, this can be considered in relatively good agreement with the CL intensity recorded in Fig.3.9.a. Fig.3.10 reveals the presence of a hexagonal defect (outlined in red) which can be spatially correlated with the centre of the feature in the panchromatic CL image in Fig.3.9.b. We note that in this case the diameter of the feature shown in the pan-CL image (Fig.3.10) is approximately 4-5  $\mu\text{m}$ , far smaller than what is observed in the EL. We expect this to be due to the different excitation methods for both SEM-CL and EL.

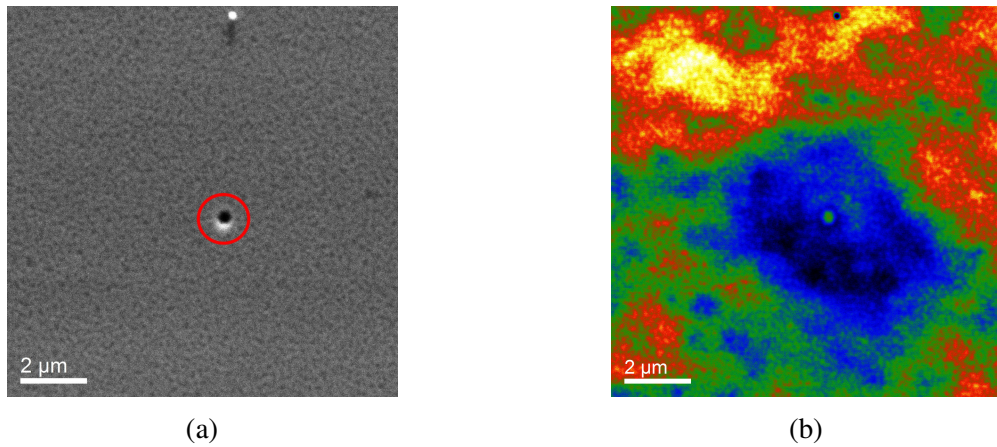


Fig. 3.10 a) SEM micrograph and b) pan-CL image of an inhomogeneity in C5608A. The pan-CL image utilises a temperature scale (blue = low, red = high).

A hyperspectral CL map of  $2 \times 2 \mu\text{m}^2$  was taken to examine the emissive properties of the defect in more detail. Fig.3.11.a. shows that as expected, the region close to the hexagonal defect exhibits low CL intensity. Interestingly, the defect also shows extremely low-energy emission relative to the background, most likely due to defect-related yellow band emission [105].

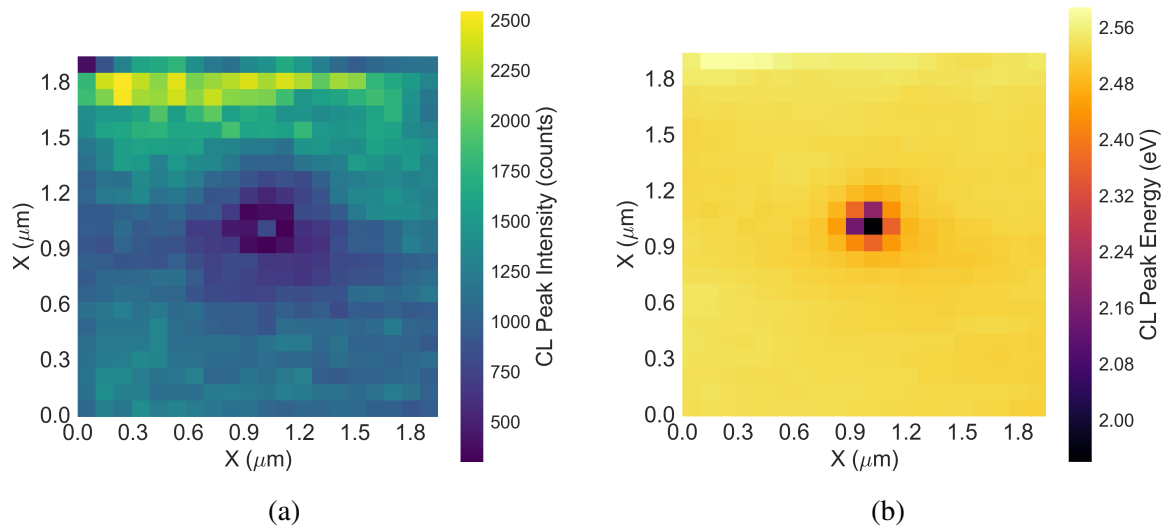


Fig. 3.11 a) CL maximum peak intensity and b) CL peak energy for the feature shown in Fig.3.10

### 3.3.3 Hexagonal Defect Structure

The structure of the hexagonal defects found at the centre of the inhomogeneities was examined following their detection using SEM-CL.

#### 3.3.3.1 Scanning Electron Microscopy

In order to achieve a higher resolution in examining the defects via SEM, an FEI Helios Nanolab 650 SEM/FIB with a schottky FEG at 5 kV and through lens detector (TLD) was used to perform high resolution SEM imaging. This is shown in Fig. 3.12.

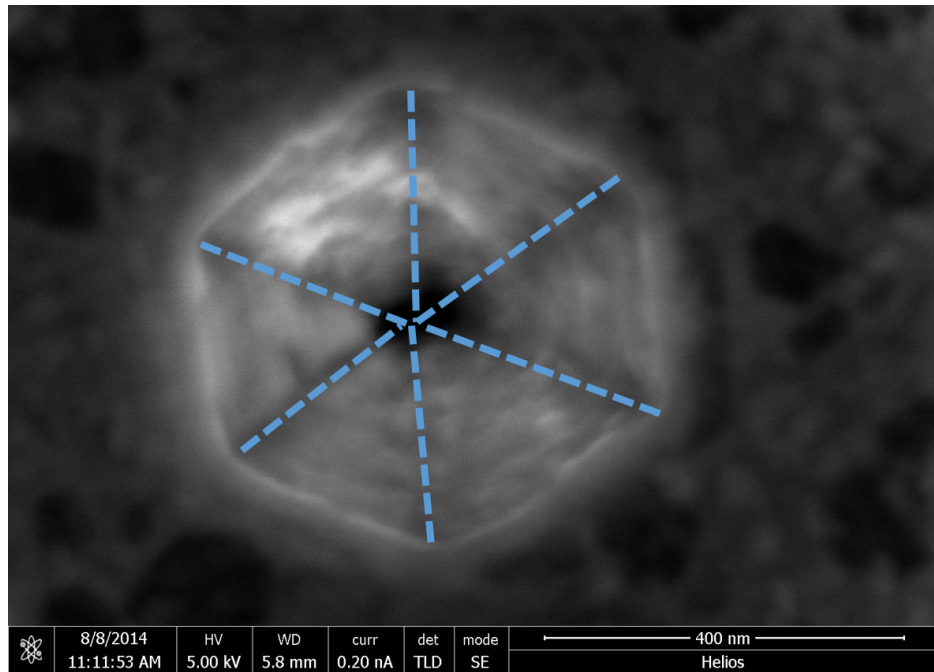


Fig. 3.12 High-resolution SEM image of a hexagonal defect located at the centre of an inhomogeneity in the EL. The vertices of the facets are delineated by dashed lines.

Most hexagonal defects located at the centre of the inhomogeneities fell within the 200-600 nm range, with some exceedingly large defects reaching up to 1  $\mu\text{m}$  in size. This is rather uncommon for hexagonal defects in III-nitrides, as the lateral size of hexagonal defects is typically sub-100 nm [106, 36].

### 3.3.3.2 Atomic Force Microscopy

The topography of the hexagonal defect was studied by AFM performed on a Veeco Dimension 3100 with RTESP tips with a nominal radius of 8 nm in intermittent contact mode. The defect shown in the SEM micrograph in Fig.3.12 is shown below in the AFM image.

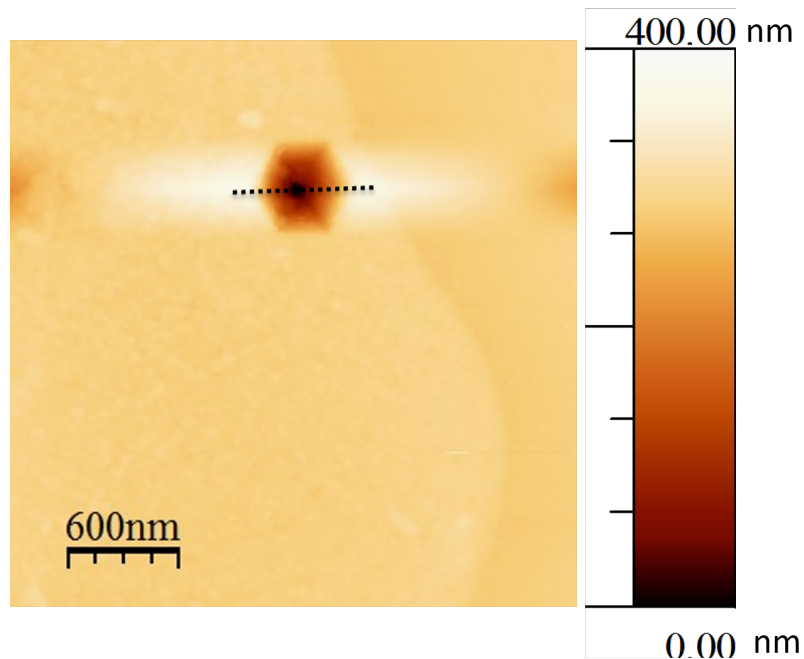


Fig. 3.13 AFM image of the hexagonal defect.

By taking a topography profile across the hexagonal defect, we can resolve the depth of the defect as well as the slope of the facets. From the profile taken in Fig.3.13 we can calculate the angle at the apex of the facets, which yields a value of approximately 60 degrees. The deviation from the ideal value of 60 degrees is expected to be due to drift during the AFM scan, causing the second facet to appear elongated and at a smore shallow angle. The raised area surrounding the pit is an artifact resulting from the large changes in depth encountered by the AFM tip during the scan, and can be reduced by reducing the scanning speed.

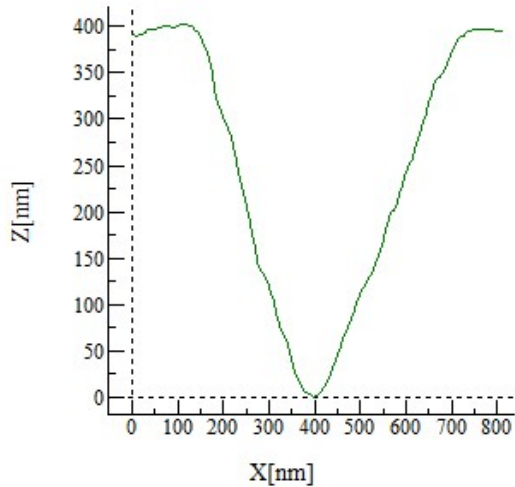


Fig. 3.14 Profile taken across the defect shown in Fig.3.13

### 3.3.3.3 TEM Lamella preparation

Preparation of TEM lamellae for the analysis of the defects requires some additional steps due to site-specific nature of the experiment. Standard FIB/SEM sample preparation methods simply require a  $2\ \mu\text{m}$  thick wedge of the sample to be extracted and thinned down to a thickness of 100-200 nm for TEM experiments. However, analysis of the defect and any associated dislocations which may be present at the apex of the inverted pyramidal shape [107, 108] requires thinning to be performed in an extremely controlled manner. A method devised by Thomas O'Hanlon at the Cambridge Centre for Gallium Nitride was utilised to perform high-precision site specific TEM sample preparation shown in Fig.3.15. A 'marker layer' consisting of a cross intersecting the apex of the defect is deposited using the electron beam, thus allowing for little damage to the unprotected sample and a higher deposition resolution than the ion beam. Following this a protective layer is then deposited using the ion beam, and a standard dual-beam lift-out method is used to extract the wedge of sample containing the defect.

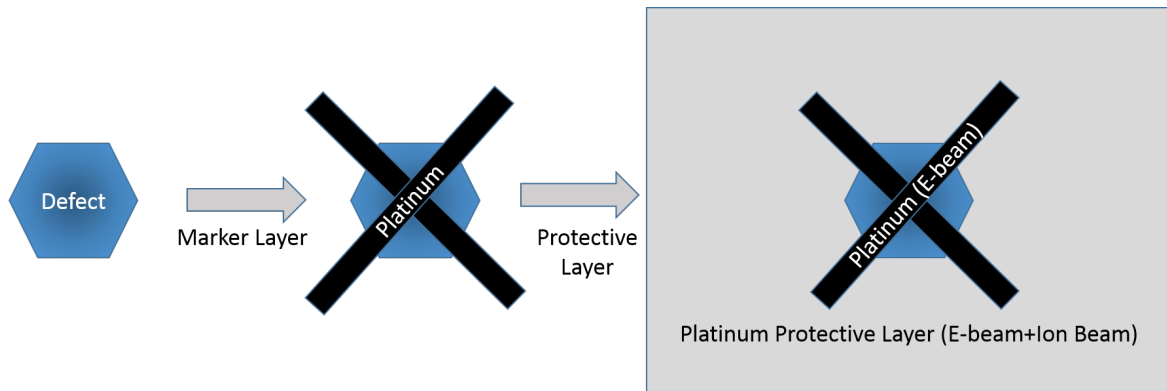


Fig. 3.15 Marker layer deposition for high precision TEM sample preparation.

The purpose of the marker layer is guide the sample thinning process. The electron beam deposited platinum provides contrast against both the sample and the ion-beam platinum in the SEM image. As the sample is imaged in cross-section during the thinning process, the distance between the marker layer 'ends' is an indicator of the proximity to the defect apex. As the defect apex is reached during the thinning process, the two marker stripes should merge into one at the intersection of the cross, as shown in Fig.3.16.

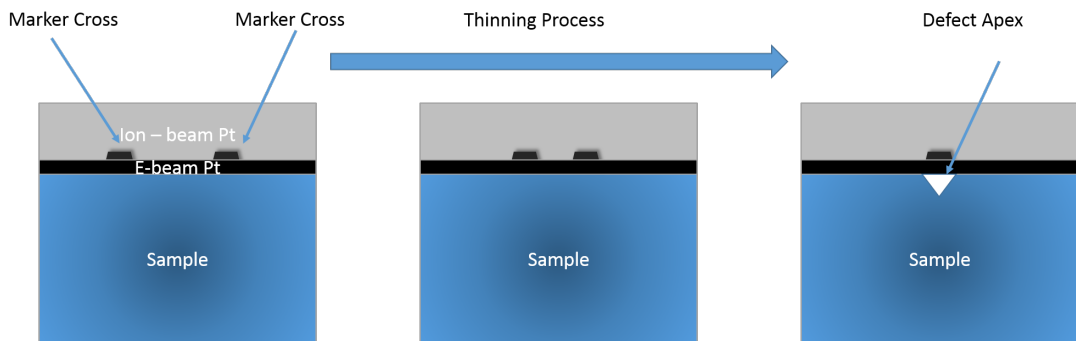


Fig. 3.16 Marker layer deposition for high precision TEM sample preparation.

A successfully thinned sample is shown in Fig.3.17.

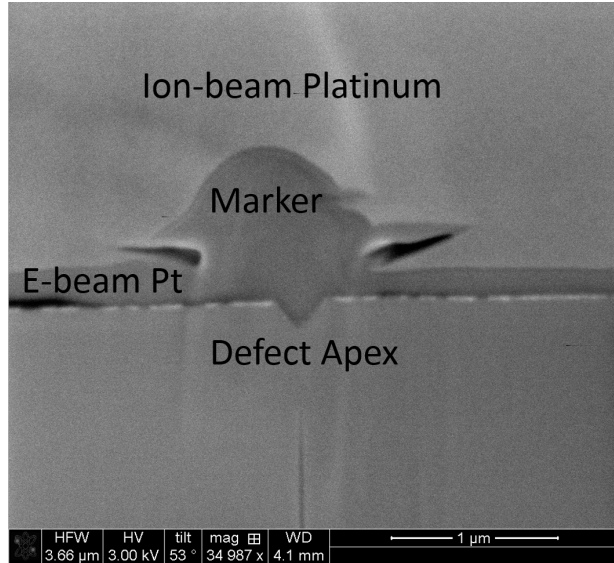


Fig. 3.17 SEM image of a prepared TEM lamella showing the marker position and defect apex.

### 3.3.3.4 Transmission Electron Microscopy

The site-specific TEM lamella prepared using the dual-beam methods, shown in Fig.3.17, was studied by HAADF-STEM performed on an FEI Osiris microscope with an extreme-FEG (X-FEG) at 200 kV. HAADF-STEM imaging of the defect reveals it originates below the MQW stack, a possible explanation for the large size of the hexagonal defects relative to those reported in literature [34, 36, 106]. We note the dark contrast in HAADF-STEM provided by the protective e-beam deposited Pt layer, which is certainly counter intuitive as Pt is a heavier element than those contained in the LED structure (Ga,In,Al and N). We believe this is due to the high concentration of C in Pt deposited by the dual-beam FIB/SEM, which is also a product of the decomposition of the organometallic precursor used for Pt deposition [109]. In contrast, we note the bright contrast from the Au-Ni *p*-contact at the surface of the LED structure, labelled in Fig.3.18, we believe that the bright feature which can be observed near the apex of the defect and running along on of the facets to the deposition of Au-Ni contact within the defect.

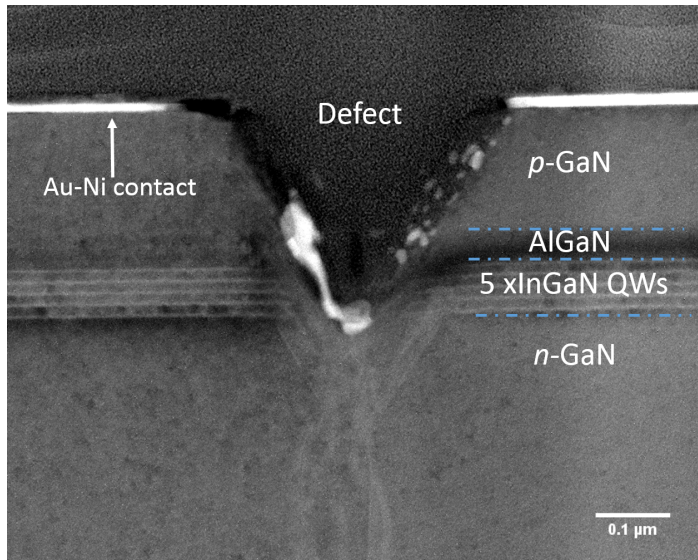


Fig. 3.18 HAADF-STEM image of a prepared TEM lamella showing defect interrupting the QW stack.

The composition of the MQW stack adjacent to the region occupied by the defect was studied using EDX-STEM, where the characteristic X-rays emitted by the sample were recorded by four silicon drift detectors which form a solid angle greater than 0.9 sr. Cliff-Lorimer analysis of the aluminium, gallium and indium was performed using HyperSpy [110] in order to quantify the ternary alloy compositions as shown in Fig.3.19. Details concerning the Cliff-Lorimer approach towards quantitative EDX-analysis can be found in [111]. K-factors for the Cliff-Lorimer analysis were provided by the detector manufacturer. Quantification consistency was tested by performing the quantification process using both Hyperspy and a custom Matlab EDX quantification script authored by Dr. James Griffiths and Dr. Spark Zhang.

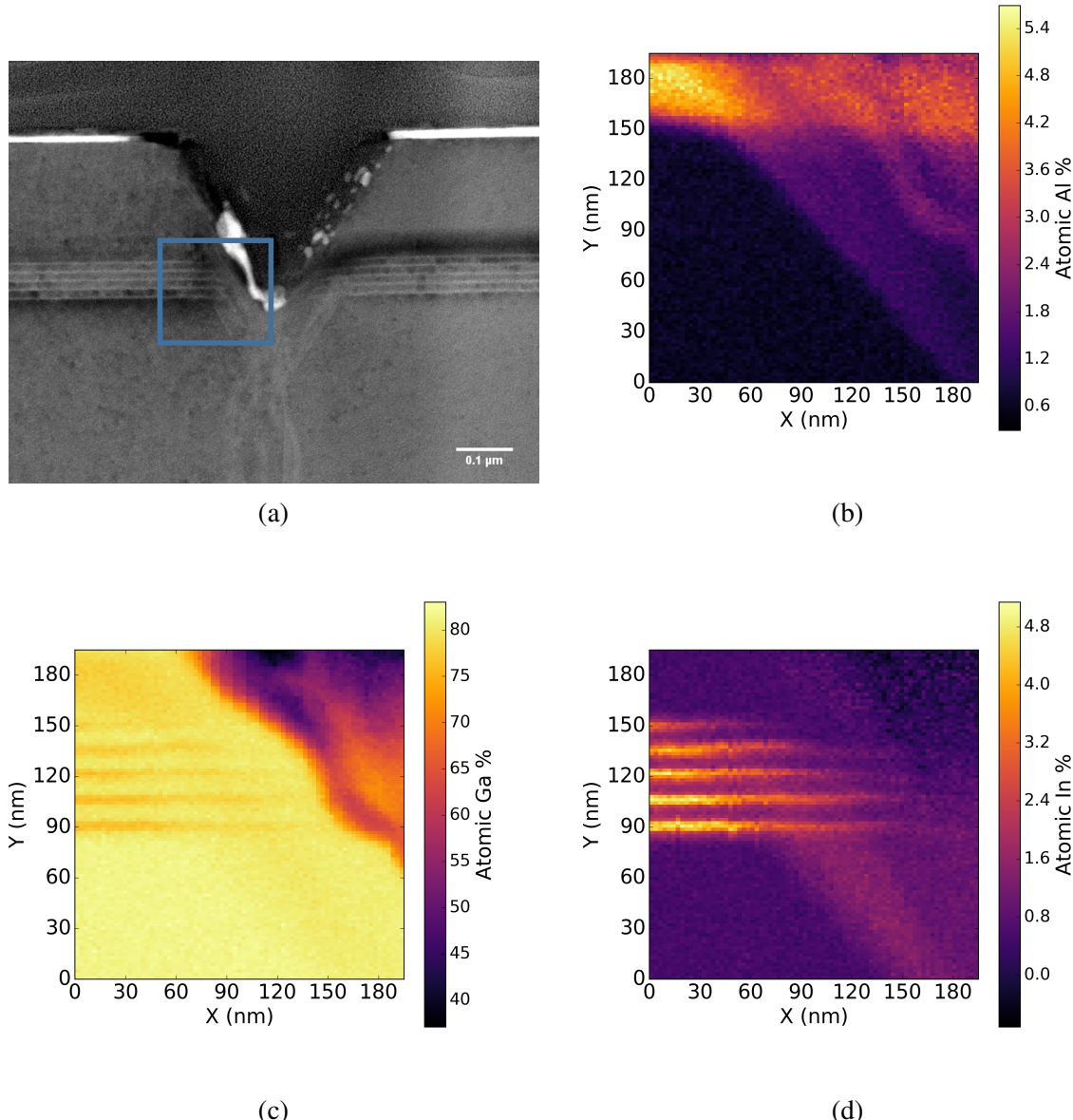


Fig. 3.19 Quantification of the ternary alloy compositions: a) HAADF-STEM image showing the region examined by EDX (blue box) b) aluminium atomic percentage, c) gallium atomic percentage and d) indium atomic percentage.

The EDS analysis shows the disruption of the QW stack by the defect, as evidenced by the apparent termination of the QW In signal in Fig.3.19.d. Additionally, the Al signal can be seen to overlap with the QW In signal, suggesting the presence of aluminium in the region disrupted by the defect. Furthermore, there is an observable indium signal originating from below the QWs. Although both the aluminium and indium atomic percentages observed in the region disrupted by the defect appear lower than expected (approximately 3 % and 2 % respectively) it is also important to consider the effect of the sample geometry in the collection of the EDX signal: due to the inverted pyramidal morphology of the defect the collected signal is expected to be reduced, and thus the atomic percentages obtained via quantification are expected to be under-estimates. In order to confirm the composition of the bright feature captured within our EDX scan, we examined the compositions for the *p*-contact material Au and Ni. Figures 3.20a. and b. show the Au and Ni atomic composition respectively, indicating that the material is likely to be a combination of both. The high Pt content over this area is likely due to projection effects as the material behind the bright feature is likely to be the protective Pt layer. We also note the presence of Cu over the sample, most likely due to deposition from the Cu TEM grid. We note that the presence of Pt and Cu over the majority of the sample may lead to errors in the accuracy of the elemental quantification, however the relative compositions should remain valid.

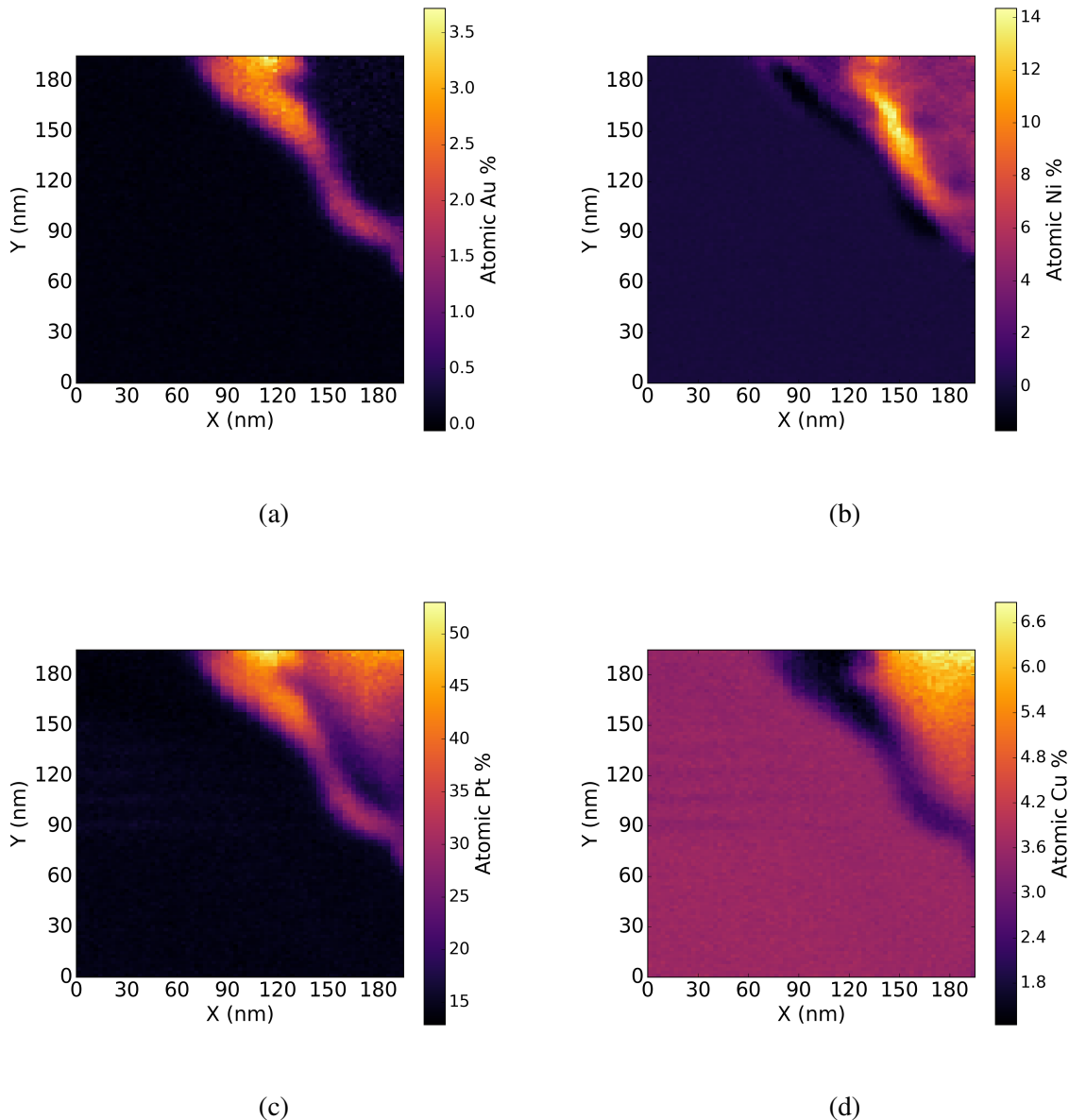


Fig. 3.20 Quantification of the metallic element compositions: a) Gold atomic percentage b) Nickel atomic percentage, c) Platinum atomic percentage and d) Copper atomic percentage.

### 3.3.4 LED Simulations

In order to investigate the manner in which changes induced by the defect could affect the EL of the LED simulations were performed by Bertand Rouet-Leduc using the APSYS simulation package, with parameters taken from J.Piprek [112]. APSYS couples a quantum-mechanical model for photon emission from the InGaN QWs in LEDs with self-consistently computed semiconductor carrier transport equations. Built-in polarization at nitride material interfaces is calculated using a second-order model described in [113]. Poisson and Schrodinger equations are solved iteratively to account for the QCSE as well as the quantum well deformation which is dependent on device bias. The carrier transport model considers a combination of band-to-band tunneling, thermionic emission at hetero-interfaces, Fermi statistics and the drift and diffusion of carriers [114]. For futher discussion of the mechanics behind the simulations of APSYS, please refer to [114].

#### 3.3.4.1 Deep Inclusion

Fig.3.21 shows the simulated LED structure with a hexagonal defect incorporated. In this case we assume the QW stack simply continues along the edge of the hexagonal defect as described in [34], as the EDX quantification reveals a detected atomic percentage of indium of approximately 4 % below the QW stack. We assume a similar geometry for the AlGaN EBL, which is expected to follow the angled facet of the defect. Thus, this set of simulations deals with what we term a 'deep' AlGaN inclusion, which is expected to penetrate below the QW stack. Although the atomic Al percentage shown in Fig.3.19.b. below the QW stack is reduced relative to the Al percentage in the EBL, this may be due to projection artifacts related to the geometry of the hexagonal defect and the thickness of the TEM lamella.

In this set of simulations, we have set the *p*-GaN doping concentration to  $3 \times 10^{19} \text{ cm}^{-3}$ , the *p*-AlGaN EBL doping to  $4 \times 10^{19} \text{ cm}^{-3}$  except on the semi-polar facets of the defect where it is set to  $1 \times 10^{19} \text{ cm}^{-3}$ .

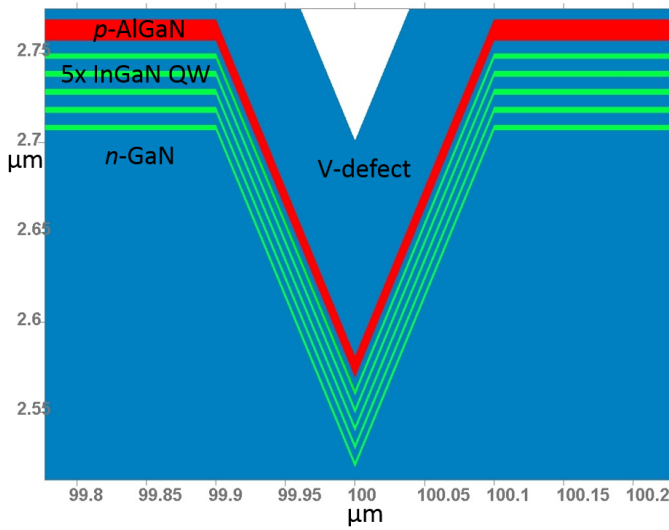


Fig. 3.21 Simulated LED structure.

The simulation results are shown in Fig.3.22.. Fig.3.22. shows a two-dimensional map of the overall radiative recombination rate in units of  $10^{28} \text{ cm}^{-3} \text{ s}^{-1}$ . It is important to note the x-axis of Fig.3.22 is enlarged relative to the y-axis for visualisation purposes. The region closest to the defect at the lowest QW (QW5) shows an increased radiative recombination rate, in agreement with the experimental observation of inhomogeneous EL, which was brighter at the location of the defects within the resolution of the hyperspectral EL data shown in Section 3.3.1.1. Fig.3.23.shows two profiles taken from Fig.3.22.a. intersecting the five QWs and indicates that the rate of radiative recombination is almost doubled in the lowest QW close to the defect when compared with a profile taken further away from the defect.

Under closer examination, Fig.3.23. demonstrates that the 'bottom' QW dominates the overall emission, particularly close to the AlGaN inclusion. We note that the distance label of the x-axis in Fig.3.23,3.24 and 3.25 is the distance from the centre of the hexagonal defect in the simulation. At QW5, which here is the label used to describe the QW closest to the substrate and furthest from the *p*-contact, we can see that the radiative recombination close to the simulated defect (at approximately 150 nm from the apex of the defect and labelled in red) is enhanced by a factor of 2 relative to the profile taken at 400 nm from the defect (in black). Interestingly QW1 and QW2 exhibit slightly lower radiative recombination close to the defect relative to the profile taken at a distance of 400 nm from the defect. The carrier concentrations shown in Figures.3.24 and 3.25 show that this is primarily due to the enhanced hole concentration in the region adjacent to the AlGaN, as the electron concentration is relatively unchanged. Thus we can ascribe the enhanced local carrier concentration to the

presence of the *p*-AlGaN, which injects holes directly into the active region. The effects of hexagonal defect-assisted carrier injection into MQW stacks have been reported by Li *et al.*, who reported that the disruption of the MQW stack by the hexagonal defect combined with thinner QBs allowed for the injection of holes up to 8 pairs of QWs away from the *p*-GaN [115]. Quan *et al.* have also suggested that hole injection via the semi-polar facets of the hexagonal defect occurs at a higher rate resulting in high radiative recombination near the defect, but larger defects may result in localised emission [116].

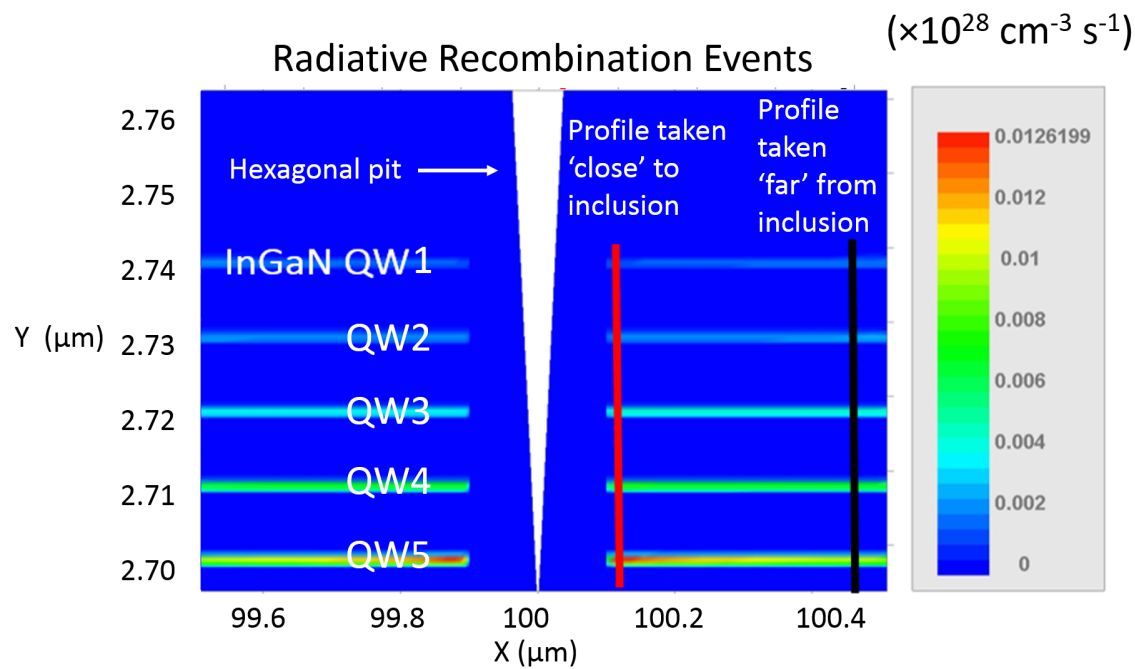


Fig. 3.22 APSYS simulation results: Radiative recombination events

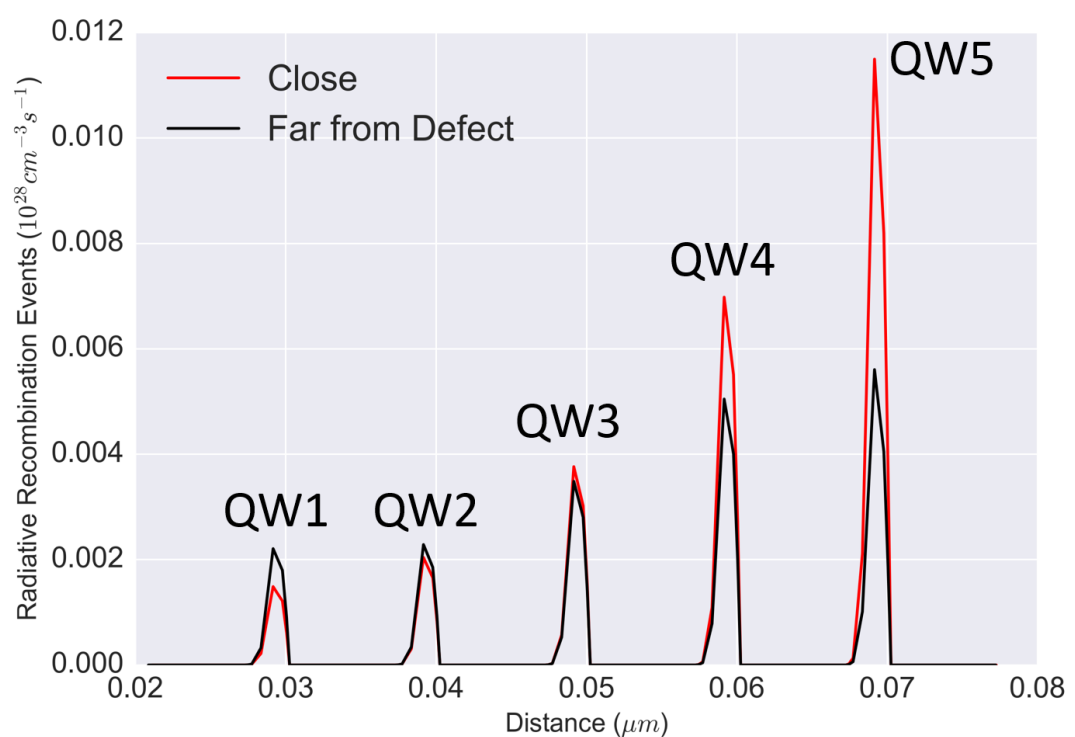


Fig. 3.23 APSYS simulation results: radiative recombination profiles

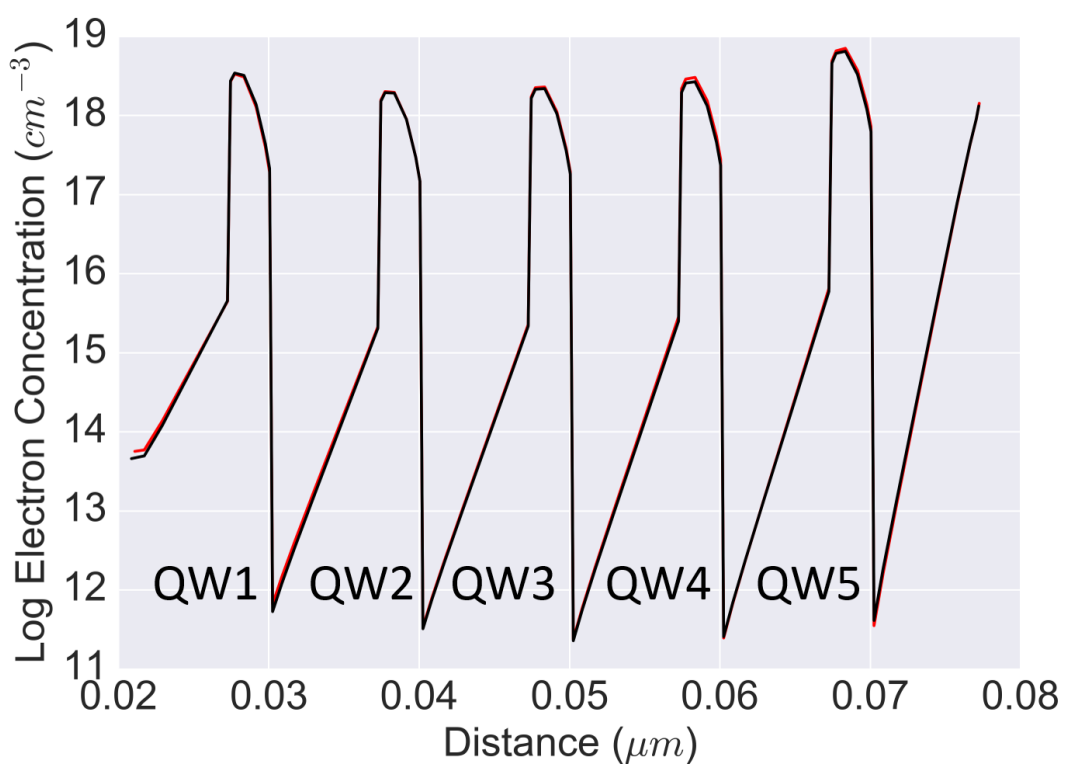


Fig. 3.24 APSYS simulation results: log electron concentration profiles

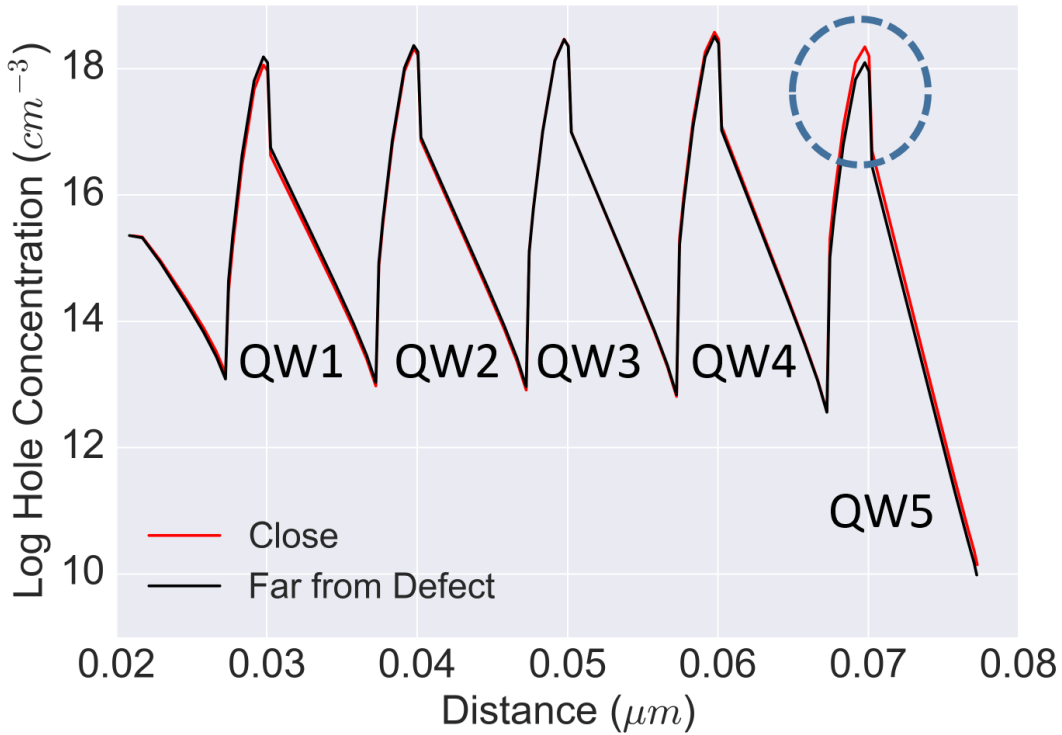


Fig. 3.25 APSYS simulation results: log hole concentration profiles

### 3.3.4.2 Shallow Inclusion

In this simulation we have simulated a structure similar to the composition maps shown in Fig.3.19. We have assumed that the AlGaN EBL may penetrate only slightly in into the QW stack due to the defect, but otherwise the rest of the disrupted region is filled with undoped GaN. The AlGaN EBL doping is set to  $5 \times 10^{18} \text{ cm}^{-3}$  with an Al content of 10%. Thus, in this case we assume no projection artifacts, as opposed to the deep Al inclusion simulated previously. The geometry used for this simulation is shown in Fig.3.26.

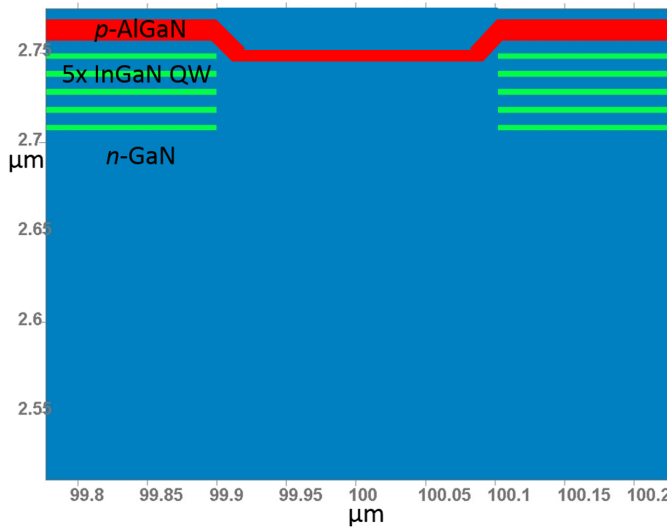


Fig. 3.26 Simulated LED structure for the shallow inclusion.

Fig.?? shows the simulation results. Fig.3.27. shows that radiative recombination is enhanced in the vicinity of the shallow inclusion, particularly in the second QW (QW2) from the EBL due to carrier injection from the semi-polar facets of the defect. Fig.3.29.c. and Fig.3.30.d. show that the hole concentration is responsible for the local enhancement in radiative recombination near the shallow inclusion as the electron concentration is mostly unchanged. Fig.3.30 show that the enhanced injection of holes results in an order of magnitude increase in radiative recombination in QW2. As such, even in the case of a 'shallow' *p*-AlGaN inclusion induced by a hexagonal defect, the injection of holes into the active region still results in enhanced emission adjacent to the defect.

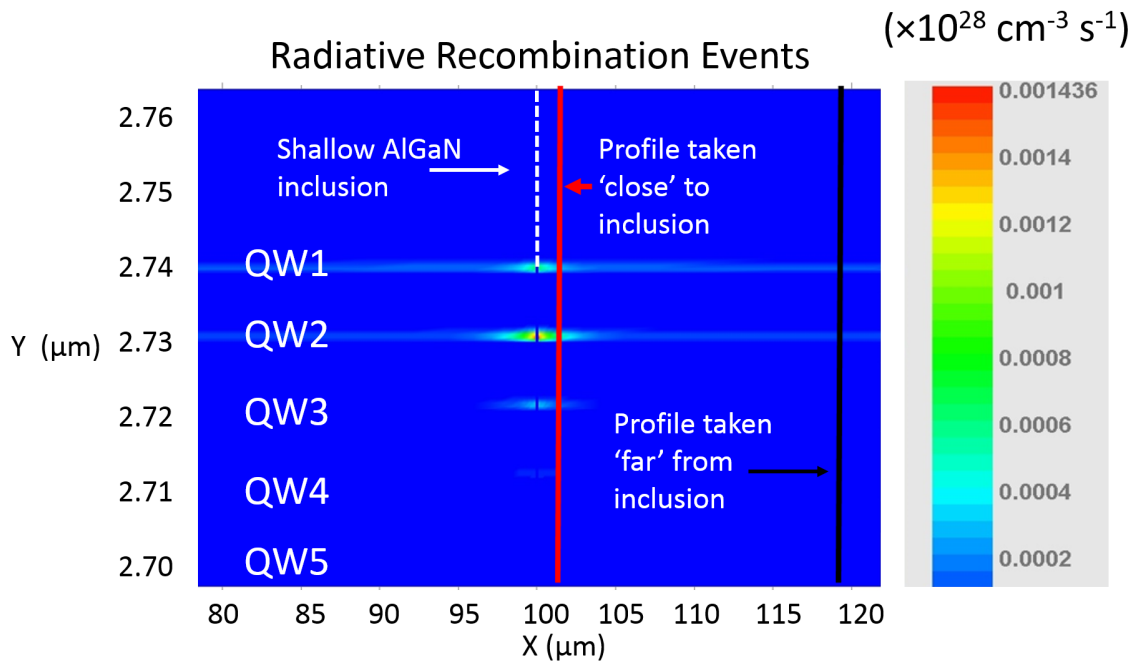


Fig. 3.27 APSYS simulation results: a) Radiative recombination events

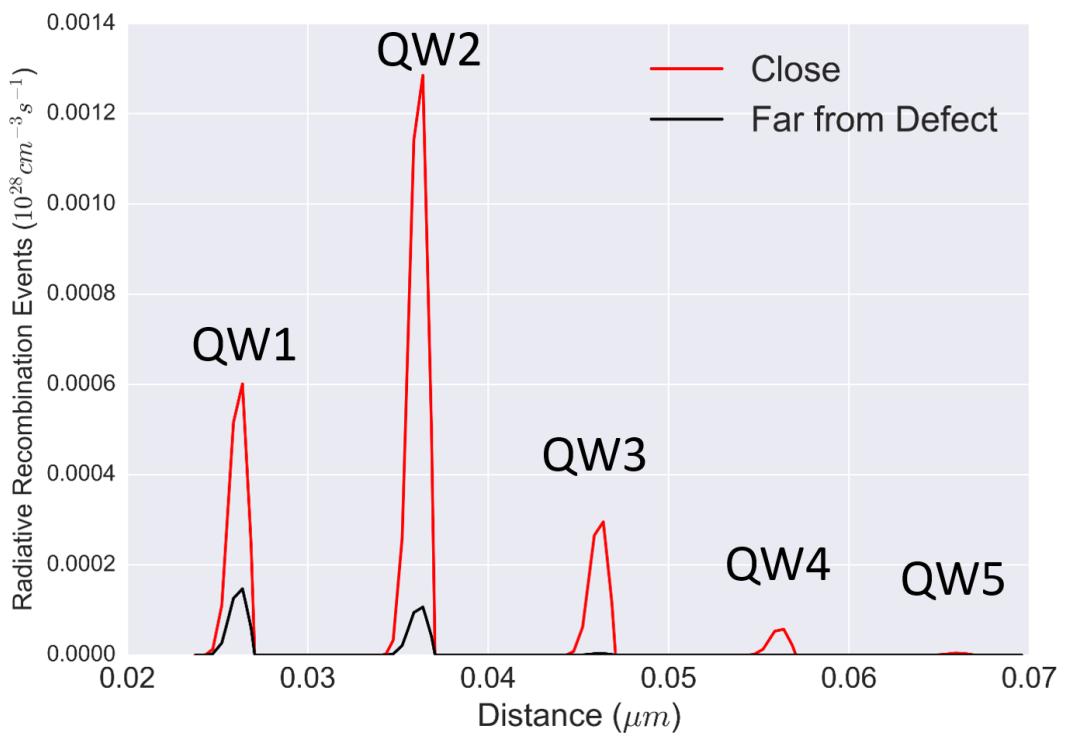


Fig. 3.28 APSYS simulation results: a) Radiative recombination events

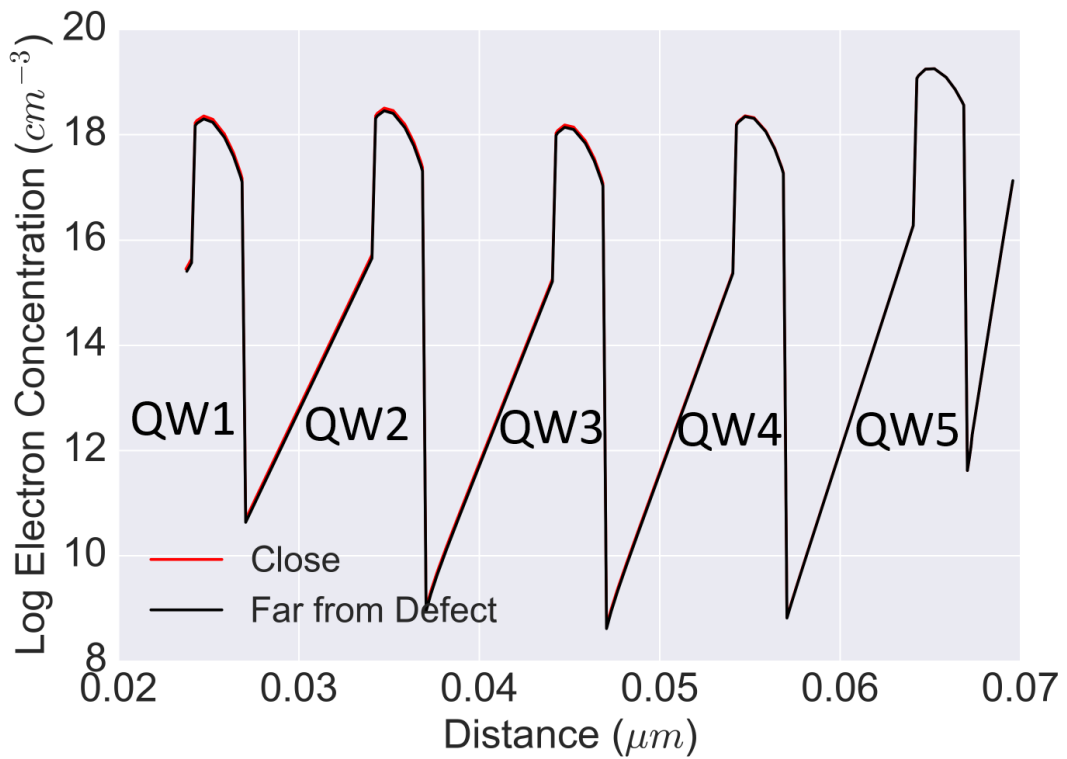


Fig. 3.29 APSYS simulation results: electron concentration

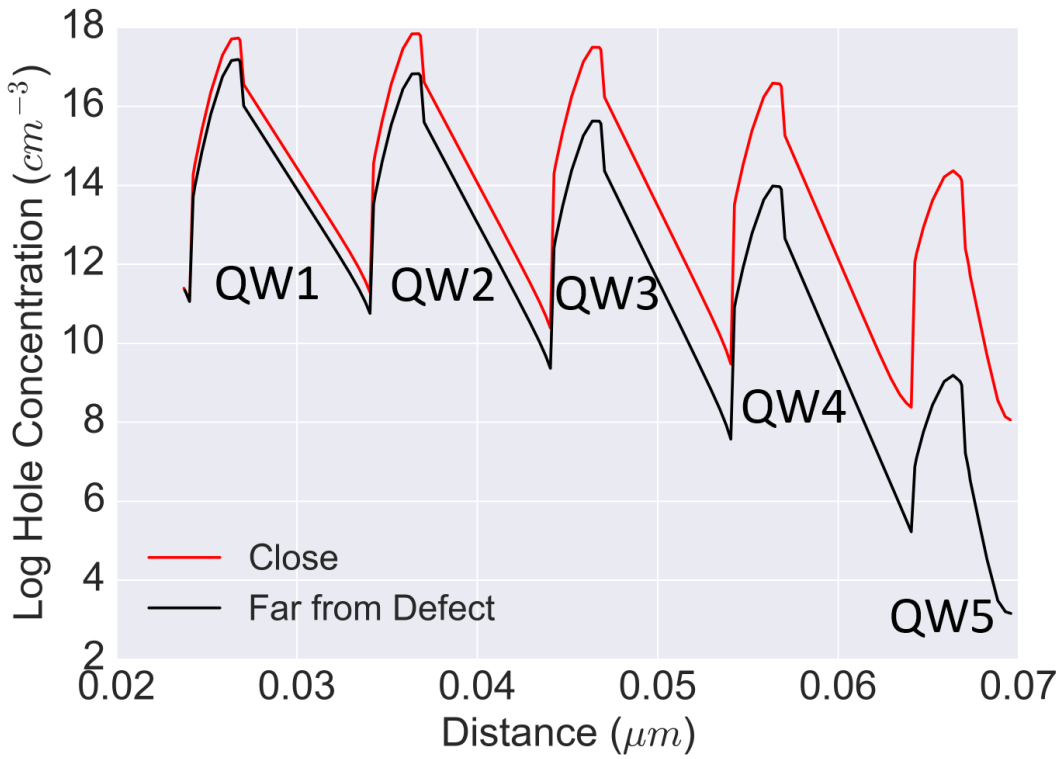


Fig. 3.30 APSYS simulation results: hole concentration

In order to reconcile the results of the simulations with the EL data, we must consider that the EL data is extracted light from the LED, rather than the emitted light.. The simulated emission pattern suggests enhanced radiative recombination within approximately  $5 \mu\text{m}$  of the hexagonal defect, however the hyperspectral EL data suggests a circular area of enhanced emission, as shown in Fig.3.5. Considering the critical angle for the light extraction from the surface of the LED due to Snell's law as shown in Fig.3.31:

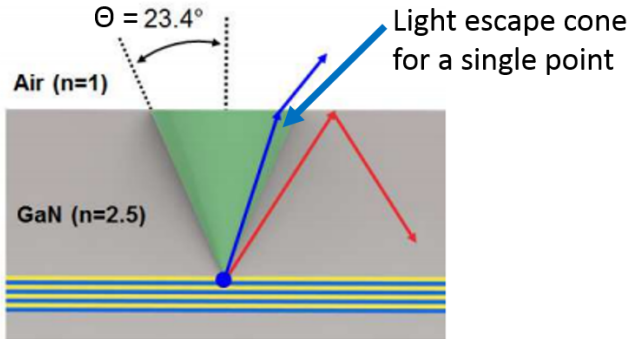


Fig. 3.31 Critical angle for an air/GaN interface [117].

We can see the extracted light is in fact a convolution of multiple light escape cones, as such despite the lack of emission from the hexagonal defect itself, we expect the EL data to appear as a singular bright area rather than a hollow area as depicted by the APSYS simulations. This is shown schematically in Fig.3.32.

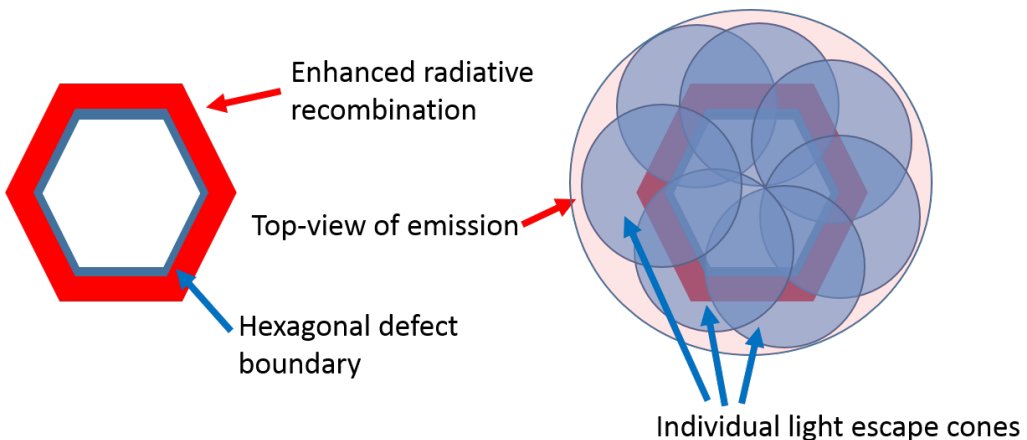


Fig. 3.32 Left: actual emission pattern surrounding the defect due to enhanced carrier injection. Right: Top-view of the emission: the hollow morphology is lost due to the convolution of multiple light escape cones surrounding the defect.

### 3.3.5 Origin of the Defect

In the previous sections we have established the cause of the inhomogeneous EL to be the presence of large hexagonal defects. However, it is also important to establish the origin of these hexagonal defects, as their elimination is the key to the production of LEDs with uniform emission, unlike those studied here.

### 3.3.5.1 Threading Dislocation Analysis

Hexagonal defects are typically associated with threading dislocations [118], as such we performed TEM on the FIB prepared lamella in order to observe threading dislocation associated with the hexagonal defects observed at the centre of inhomogeneities in the EL. The TEM image is shown in Fig. 3.33. Interestingly, rather than a single TD, we can observe a 'bundle' of dislocations associated with the defect with several 'loops' also apparent.

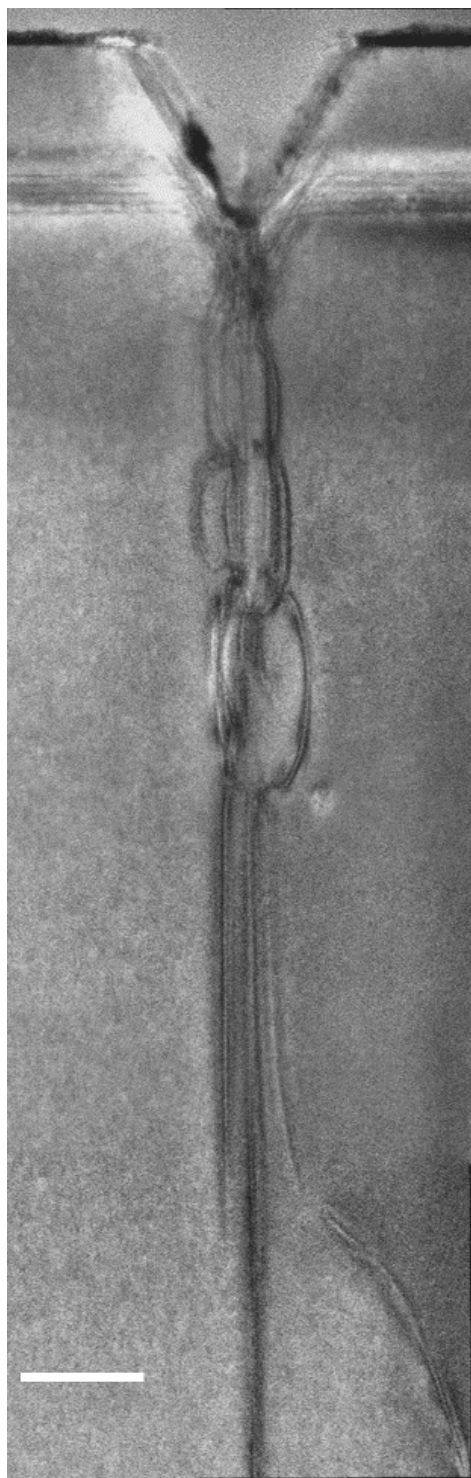


Fig. 3.33 TEM image viewed along the  $(10\bar{1}0)$  direction of the dislocations associated with the hexagonal defect shown in Fig.3.18. The scale bar corresponds to a length of 200 nm.

In order to characterise the dislocations shown in Fig.3.33, WBDF-TEM was performed. The results are shown in Fig.3.34.

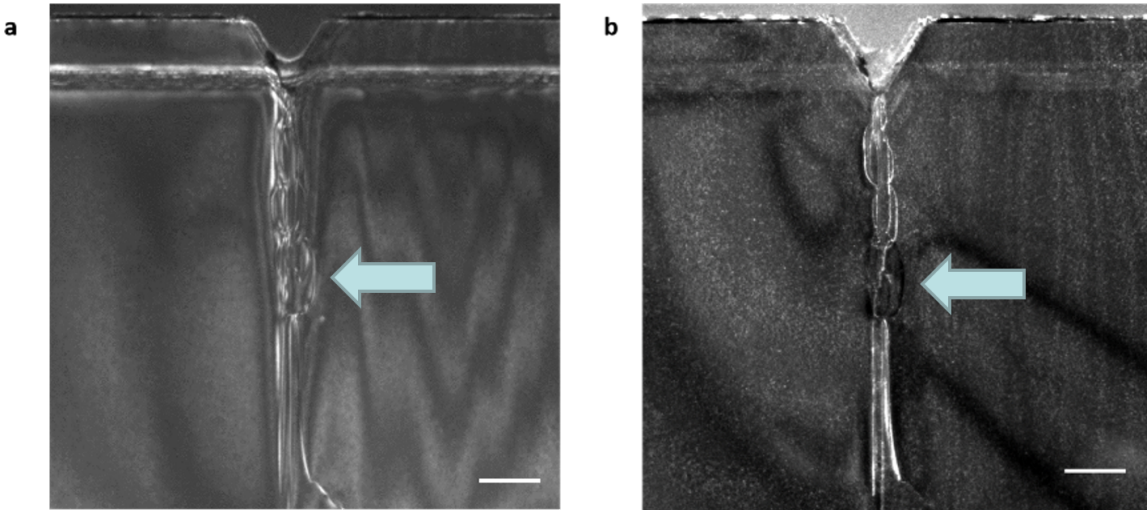


Fig. 3.34 WBDF-TEM of TDs associated with the hexagonal defect under a)  $\mathbf{g} = \langle 11\bar{2}0 \rangle$  and b)  $\mathbf{g} = \langle 0001 \rangle$ . The scale bar corresponds to a length of 150 nm.

Fig.3.34 shows that the majority of TDs associated with the pit are mixed in nature, with some exceptions such as the 'dislocation loop' which shows no contrast under when viewed under the condition  $\mathbf{g} = \langle 0001 \rangle$ . Nonetheless, the number of TDs associated with a single defect here is astonishing.

The bundle of TDs observed here could potentially be attributed to the vertical side facets in GaN islands during the initial growth of the GaN template on sapphire. Datta *et al.* showed that threading dislocations associated with basal plane stacking faults are located at coalescence boundaries between two GaN grains, and can open up into hexagonal defects at the surface, as shown in Fig.3.35 [119]. In order to avoid GaN grains with vertical side facets, Datta *et al.* suggest initialising epilayer growth at a low V/III ratio or increased pressure as these conditions favour the formation of GaN islands with inclined side facets[120, 121], thus allowing TDs to bend laterally during film coalescence rather than propagate upwards towards the epilayer surface and form hexagonal defects.

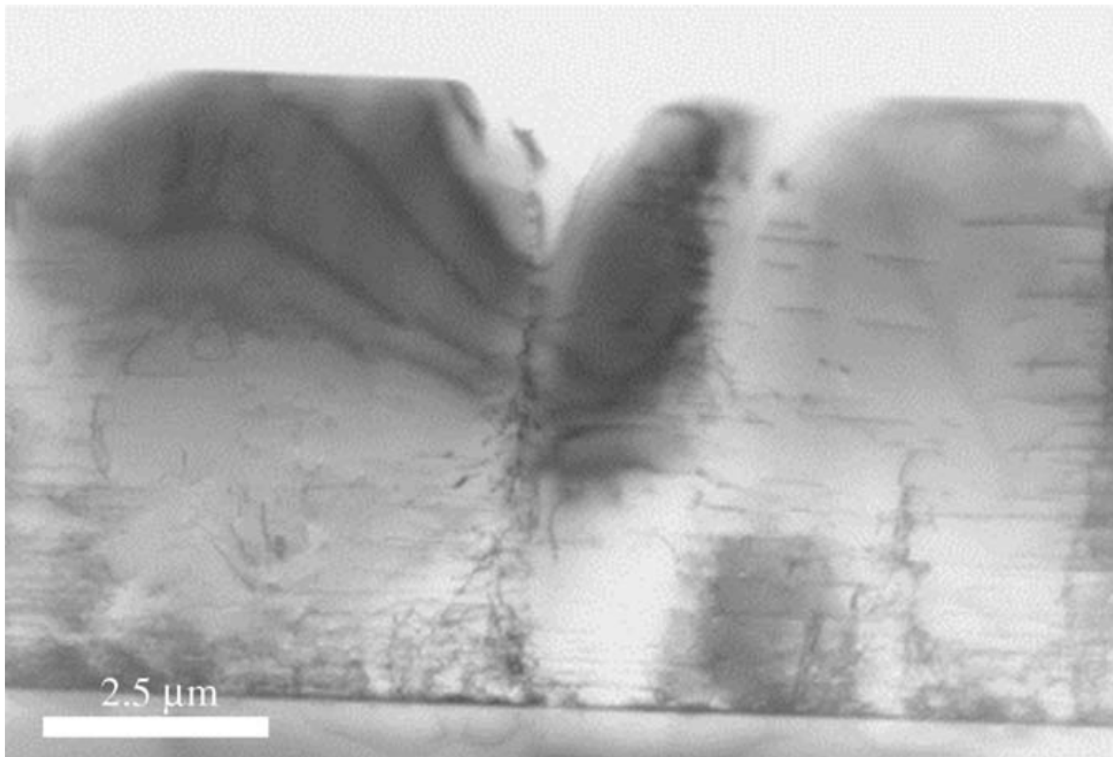


Fig. 3.35 BF-TEM image of a coalescence boundary between two GaN grains and associated threading dislocations opening up into a hexagonal defect [119].

### 3.4 Conclusion

First and foremost we have utilised a host of microscopy techniques to identify the cause of inhomogeneous EL in III-nitride LEDs. Hyperspectral EL mapping was performed over a set of inhomogeneities in order to determine their spectral properties. Using this data, the inhomogeneities were established to be blueshifted and have a larger emission FWHM. Further current dependent EL-measurements revealed that the inhomogeneities exhibited emissive properties consistent with higher local carrier concentration.

SEM-based techniques were used to further elucidate the properties of the inhomogeneities. Panchromatic CL was used to reveal dark regions surrounding the inhomogeneities, as well as hexagonal defects at the centre of the inhomogeneities.

A FIB-based technique to deposit marker layers was used in order to produce a TEM lamella through the apex of a hexagonal defect at the centre of an inhomogeneity. This allowed for STEM-EDX mapping of the region surrounding the defect apex, revealing the presence of Al from the AlGaN EBL in the active region.

APSYS simulations were performed in order to examine the effect of AlGaN penetrating

within the active layer for both a 'deep' (penetrating all the way through to the  $n$ -GaN) and 'shallow' (penetrating down to only the first QW) inclusion. Both sets of simulations demonstrated that the  $p$ -doped AlGaN can indeed enhance local EL through the injection of holes into the active region, thus establishing the presence of  $p$ -doped material within the active region due to the hexagonal defect as a likely cause for the inhomogeneities observed. Conventional TEM techniques were used to observe a bundle of TDs associated with the hexagonal defect, establishing that the defects are likely due to sub-optimal template growth conditions. Datta *et al.* suggest the presence of TD bundles at coalescence boundaries can be ascribed to GaN grains with vertical side facets. As such, template growth in a low V/III ratio or increased pressure is necessary to encourage the formation of GaN islands with inclined  $\{1\bar{1}01\}$  or  $\{11\bar{2}2\}$  is necessary to avoid vertically propagating TD bundles [119].

### 3.5 Future Work

We have established the root cause of the EL inhomogeneity as the presence of hexagonal defects, however not all inhomogeneities observed in the panchromatic CL were associated with detectable defects in the SEM. This may be due to several reasons: the hexagonal defects may have 'filled' during the growth process, or are of much smaller size ( $<50$  nm [106, 36]) and are thus not easily detectable due to the presence of the Ni/Au  $p$ -contact. Cross-sectional TEM of an inhomogeneity without a large defect at the centre may provide the answer to this question. The presence of the V-defects as 'leakage' pathways has been well supported in literature [115, 116], however it is possible the bundle of dislocations associated with the defect may provide additional leakage pathways. Conductive-AFM may serve to provide a clearer image of the conductive properties of the defects.



# References

- [1] C. J. Humphreys, “USE Solid-State Lighting,” *MRS Bulletin*, vol. 33, no. April, pp. 459–471, 2008.
- [2] S. Nakamura, T. Mukai, and M. Senoh, “High-Power GaN P-N Junction Blue-Light-Emitting Diodes,” *Japanese Journal of Applied Physics*, vol. 30, no. 12A, pp. 1998–2001, 1991.
- [3] S. Najda, P. Perlin, L. Marona, M. Leszczy, R. Czernecki, S. Watson, A. E. Kelly, A. Malcolm, P. Blanchard, and H. White, “Novel laser diode technology for free-space communications,” *SPIE*, pp. 10–12, 2015.
- [4] H. Berlien, H. Breuer, G. Müller, N. Krasner, T. Okunata, and D. Sliney, *Applied Laser Medicine*. Springer Berlin Heidelberg, 2012.
- [5] S. Kako, C. Santori, K. Hoshino, S. Götzinger, Y. Yamamoto, and Y. Arakawa, “A gallium nitride single-photon source operating at 200 K.,” *Nature materials*, vol. 5, pp. 887–92, nov 2006.
- [6] S. E. Bennett, “Dislocations and their reduction in GaN,” *Materials Science and Technology*, vol. 26, no. 9, pp. 1017–1028, 2010.
- [7] E. T. Yu, X. Z. Dang, P. M. Asbeck, S. S. Lau, and G. J. Sullivan, “Spontaneous and piezoelectric polarization effects in III-nitride heterostructures,” *Journal of Vacuum Science & Technology B: Microelectronics and Nanometer Structures*, vol. 17, p. 1742, 1999.
- [8] I. Vurgaftman and J. R. Meyer, “Band parameters for nitrogen-containing semiconductors,” *Journal of Applied Physics*, vol. 94, no. 6, pp. 3675–3696, 2003.
- [9] M. E. Vickers, M. J. Kappers, T. M. Smeeton, E. J. Thrush, J. S. Barnard, and C. J. Humphreys, “Determination of the indium content and layer thicknesses in InGaN/GaN quantum wells by x-ray scattering,” *Journal of Applied Physics*, vol. 94, no. 3, pp. 1565–1574, 2003.
- [10] F. Scholz, “Semipolar GaN grown on foreign substrates: a review,” *Semiconductor Science and Technology*, vol. 27, p. 024002, feb 2012.
- [11] J. Wu, W. Walukiewicz, K. M. Yu, J. W. Ager, E. E. Haller, H. Lu, and W. J. Schaff, “Small band gap bowing in  $In_{1-x}Ga_xN$  alloys,” *Applied Physics Letters*, vol. 80, no. 25, pp. 4741–4743, 2002.

- [12] M. D. McCluskey, C. G. Van de Walle, L. T. Romano, B. S. Krusor, and N. M. Johnson, “Effect of composition on the band gap of strained  $In_xGa_{1-x}N$  alloys,” *Journal of Applied Physics*, vol. 93, no. 7, pp. 4340–4342, 2003.
- [13] P. G. Moses and C. G. Van De Walle, “Band bowing and band alignment in InGaN alloys,” *Applied Physics Letters*, vol. 96, no. 2, pp. 2–5, 2010.
- [14] T. J. Puchtler, A. Woolf, T. Zhu, D. Gachet, E. L. Hu, and R. A. Oliver, “Effect of Threading Dislocations on the Quality Factor of InGaN/GaN Microdisk Cavities,” *ACS Photonics*, vol. 2, pp. 137–143, 2015.
- [15] C. X. Ren, “Polarisation fields in III-nitrides: effects and control,” *Materials Science and Technology*, vol. 00, no. 0, p. 1743284715Y.000, 2015.
- [16] O. Ambacher and J. Majewski, “Pyroelectric properties of Al (In) GaN/GaN hetero- and quantum well structures,” *Journal of physics: D*, vol. 3399, 2002.
- [17] M. Sumiya and S. Fuke, “Review of polarity determination and control of GaN,” *MRS Internet Journal of Nitride Semiconductor Research*, vol. 9, no. 1, pp. 1–32, 2004.
- [18] C. Wood and D. Jena, *Polarization Effects in Semiconductors: From Ab Initio Theory to Device Applications*. Springer, 2007.
- [19] J. E. R. Miguel, C. J. Gladys, and O. L. César, “Computational calculation of the electronic and magnetic properties of 1x1-MN / GaN ( M = V , Cr and Mn ) multilayers,” *International Journal of Physical Sciences*, vol. 9, no. 24, pp. 538–544, 2014.
- [20] V. Fiorentini, F. Bernardini, F. D. Sala, A. D. Carlo, P. Lugli, and T. Vergata, “Effects of macroscopic polarization in III-V nitride multiple quantum wells,” *Physical Review B*, vol. 60, no. 12, pp. 8849–8858, 1999.
- [21] S. F. Chichibu, A. Uedono, T. Onuma, B. A. Haskell, A. Chakraborty, T. Koyama, P. T. Fini, S. Keller, S. P. Denbaars, J. S. Speck, U. K. Mishra, S. Nakamura, S. Yamaguchi, S. Kamiyama, H. Amano, I. Akasaki, J. Han, and T. Sota, “Origin of defect-insensitive emission probability in In-containing (Al,In,Ga)N alloy semiconductors.,” *Nature materials*, vol. 5, pp. 810–6, oct 2006.
- [22] J. H. Ryou, P. D. Yoder, J. Liu, Z. Lochner, H. S. Kim, S. Choi, H. J. Kim, and R. D. Dupuis, “Control of quantum-confined stark effect in InGaN-based quantum wells,” *IEEE Journal on Selected Topics in Quantum Electronics*, vol. 15, no. 4, pp. 1080–1091, 2009.
- [23] M. A. Reschchikov and H. Morkoç, “Luminescence properties of defects in GaN,” *Journal of Applied Physics*, vol. 97, no. 6, 2005.
- [24] H. Strite, S., Morkoç, “GaN, AlN, and InN: A review,” *Journal of Vacuum Science & Technology B*, vol. 10, no. 4, pp. 1237–1266, 1992.
- [25] X. Ning and F. Chien, “Growth defects in GaN films on sapphire: The probable origin of threading dislocations,” *Journal of materials* . . . , no. 0001, 1996.

- [26] M. A. Moram, C. S. Ghedia, D. V. S. Rao, J. S. Barnard, Y. Zhang, M. J. Kappers, and C. J. Humphreys, “On the origin of threading dislocations in GaN films,” *Journal of Applied Physics*, vol. 106, no. 7, p. 073513, 2009.
- [27] R. A. Oliver, M. J. Kappers, C. McAleese, R. Datta, J. Sumner, and C. J. Humphreys, “The origin and reduction of dislocations in Gallium Nitride,” *Journal of Materials Science: Materials in Electronics*, vol. 19, pp. 208–214, mar 2008.
- [28] L. Z.-Y. Liu, *Advanced Transmission Electron Microscopy of GaN-based Materials and Devices*. PhD thesis, University of Cambridge, 2011.
- [29] J. Lahnemann, U. Jahn, O. Brandt, T. Flissikowski, P. Dogan, and H. T. Grahn, “Luminescence associated with stacking faults in GaN,” *Journal of Physics D: Applied Physics*, vol. 47, no. 42, p. 423001, 2014.
- [30] W. Rieger, R. Dimitrov, D. Brunner, E. Rohrer, O. Ambacher, and M. Stutzmann, “Defect-related optical transitions in GaN,” *Physical Review B*, vol. 54, no. 24, p. 17596, 1996.
- [31] Y. Rebane, Y. Shreter, and M. Albrecht, “Stacking Faults as Quantum Wells for Excitons in Wurtzite GaN,” *Physica Status Solidi (a)*, vol. 164, no. 141, 1997.
- [32] J. Lahnemann, O. Brandt, U. Jahn, C. Pfüller, C. Roder, P. Dogan, F. Grosse, A. Belabbes, F. Bechstedt, A. Trampert, and L. Geelhaar, “Direct experimental determination of the spontaneous polarization of GaN,” *Physical Review B*, vol. 86, pp. 1–5, 2012.
- [33] G. Nogues, T. Auzelle, M. Den Hertog, B. Gayral, and B. Daudin, “Cathodoluminescence of stacking fault bound excitons for local probing of the exciton diffusion length in single GaN nanowires,” *Applied Physics Letters*, vol. 104, p. 102102, mar 2014.
- [34] A. Hangleiter, F. Hitzel, C. Netzel, D. Fuhrmann, U. Rossow, G. Ade, and P. Hinze, “Suppression of nonradiative recombination by V-shaped pits in GaInN/GaN quantum wells produces a large increase in the light emission efficiency,” *Physical Review Letters*, vol. 95, no. 12, pp. 1–4, 2005.
- [35] S. H. Han, D. Y. Lee, H. W. Shim, J. Wook Lee, D. J. Kim, S. Yoon, Y. Sun Kim, and S. T. Kim, “Improvement of efficiency and electrical properties using intentionally formed V-shaped pits in InGaN/GaN multiple quantum well light-emitting diodes,” *Applied Physics Letters*, vol. 102, no. 25, 2013.
- [36] H.-L. Tsai, T.-Y. Wang, J.-R. Yang, C.-C. Chuo, J.-T. Hsu, Z.-C. Feng, and M. Shiojiri, “Observation of V Defects in Multiple InGaN/GaN Quantum Well Layers,” *Materials Transactions*, vol. 48, no. 5, pp. 894–898, 2007.
- [37] S. Christopoulos, G. B. H. von Högersthal, A. J. D. Grundy, P. G. Lagoudakis, A. V. Kavokin, J. J. Baumberg, G. Christmann, R. Butté, E. Feltin, J.-F. Carlin, and N. Grandjean, “Room-Temperature Polariton Lasing in Semiconductor Microcavities,” *Physical Review Letters*, vol. 98, no. 12, p. 126405, 2007.
- [38] K. J. Vahala, “Optical microcavities,” *Nature*, vol. 424, no. 6950, pp. 839–846, 2003.

- [39] A. F. Jarjour, R. A. Taylor, R. A. Taylor, M. J. Kappers, C. J. Humphreys, and A. Tahraoui, “Cavity-enhanced blue single-photon emission from a single InGaN/GaN quantum dot,” *Applied Physics Letters*, vol. 91, no. 5, p. 052101, 2007.
- [40] I. Aharonovich, A. Woolf, K. J. Russell, T. Zhu, N. Niu, M. J. Kappers, R. A. Oliver, and E. L. Hu, “Low threshold, room-temperature microdisk lasers in the blue spectral range,” *Applied Physics Letters*, vol. 103, no. 2, p. 021112, 2013.
- [41] G. Malpuech, A. Di Carlo, A. Kavokin, J. J. Baumberg, M. Zamfirescu, and P. Lugli, “Room-temperature polariton lasers based on GaN microcavities,” *Applied Physics Letters*, vol. 81, no. 3, pp. 412–414, 2002.
- [42] A. Imamoglu, D. Awschalom, G. Burkard, D. P. DiVincenzo, D. Loss, M. Sherwin, and a. Small, “Quantum information processing using quantum dot spins and cavity QED,” *Physical Review Letters*, vol. 83, no. 20, pp. 4204–4207, 1999.
- [43] K. Hennessy, A. Badolato, M. Winger, D. Gerace, M. Atatüre, S. Gulde, S. Fält, E. L. Hu, and A. Imamoglu, “Quantum nature of a strongly coupled single quantum dot-cavity system,” *Nature*, vol. 445, no. 7130, pp. 896–899, 2007.
- [44] A. C. Tamboli, E. D. Haberer, R. Sharma, K. H. Lee, S. Nakamura, and E. L. Hu, “Room-temperature continuous-wave lasing in GaN/InGaN microdisks,” *Nature Photonics*, vol. 1, pp. 61–64, jan 2007.
- [45] S. Chang, N. B. Rex, R. K. Chang, G. Chong, and L. J. Guido, “Stimulated emission and lasing in whispering-gallery modes of GaN microdisk cavities,” *Applied Physics Letters*, vol. 75, no. 2, p. 166, 1999.
- [46] E. D. Haberer, R. Sharma, C. Meier, A. R. Stonas, S. Nakamura, S. P. DenBaars, and E. L. Hu, “Free-standing, optically pumped, GaN/InGaN microdisk lasers fabricated by photoelectrochemical etching,” *Applied Physics Letters*, vol. 85, no. 22, p. 5179, 2004.
- [47] D. Simeonov, E. Feltin, A. Castiglia, A. Castiglia, J. F. Carlin, R. Butte, and N. Grandjean, “High quality nitride based microdisks obtained via selective wet etching of AlInN sacrificial layers,” *Applied Physics Letters*, vol. 92, no. 17, pp. 2008–2010, 2008.
- [48] E. Yablonovitch, “Inhibited Spontaneous Emission in Solid-State Physics and Electronics,” *Physical Review Letters*, vol. 58, no. 20, pp. 2059–2062, 1987.
- [49] S. John, “Strong localization of photons in certain disordered dielectric superlattices,” *Physical Review Letters*, vol. 58, no. 23, pp. 2486–2489, 1987.
- [50] K. Ishizaki, M. Koumura, K. Suzuki, K. Gondaira, and S. Noda, “Realization of three-dimensional guiding of photons in photonic crystals,” *Nature Photonics*, vol. 7, no. 2, pp. 133–137, 2013.
- [51] A. Tandaechanurat, S. Ishida, D. Guimard, M. Nomura, S. Iwamoto, and Y. Arakawa, “Lasing oscillation in a three-dimensional photonic crystal nanocavity with a complete bandgap,” *Nature Photonics*, vol. 5, no. 2, pp. 91–94, 2011.

- [52] Y. Gong and J. Vukovic, "Photonic crystal cavities in silicon dioxide," *Applied Physics Letters*, vol. 96, no. 3, pp. 2009–2011, 2010.
- [53] P. B. Deotare, M. W. McCutcheon, I. W. Frank, M. Khan, and M. Lončar, "High quality factor photonic crystal nanobeam cavities," *Applied Physics Letters*, vol. 94, no. 12, pp. 8–11, 2009.
- [54] M. Notomi, E. Kuramochi, and H. Taniyama, "Ultrahigh-Q nanocavity with 1D periodicity," *Conference Proceedings - Lasers and Electro-Optics Society Annual Meeting-LEOS*, vol. 16, no. 15, pp. 689–690, 2008.
- [55] P. Lalanne and J. P. Hugonin, "Bloch-Wave Engineering for High-Q, Small-V Microcavities," *IEEE Journal of Quantum Electronics*, vol. 39, no. 11, pp. 1430–1438, 2003.
- [56] N. V. Triviño, R. Butté, J.-F. Carlin, and N. Grandjean, "Continuous Wave Blue Lasing in III-Nitride Nanobeam Cavity on Silicon," *Nano Letters*, vol. 15, no. 2, pp. 1259–1263, 2015.
- [57] N. Niu, A. Woolf, D. Wang, T. Zhu, Q. Quan, R. A. Oliver, and E. L. Hu, "Ultra-low threshold gallium nitride photonic crystal nanobeam laser," *Applied Physics Letters*, vol. 106, no. 23, p. 231104, 2015.
- [58] M. Arita, S. Ishida, S. Kako, S. Iwamoto, and Y. Arakawa, "AlN air-bridge photonic crystal nanocavities demonstrating high quality factor," *Applied Physics Letters*, vol. 91, no. 5, p. 051106, 2007.
- [59] W. H. P. Pernice, C. Xiong, C. Schuck, and H. X. Tang, "High-Q aluminum nitride photonic crystal nanobeam cavities," *Applied Physics Letters*, vol. 100, no. 9, 2012.
- [60] A. Bao, "Group iii-nitride nanowires," *Materials Science and Technology*, vol. 0, no. 0, pp. 1–12, 2016.
- [61] S. Arafat, X. Liu, and Z. Mi, "Review of recent progress of III-nitride nanowire lasers," *Journal of Nanophotonics*, vol. 7, no. 1, pp. 074599–074599, 2013.
- [62] J. C. Johnson, H.-J. Choi, K. P. Knutsen, R. D. Schaller, P. Yang, and R. J. Saykally, "Single gallium nitride nanowire lasers," *Nature materials*, vol. 1, no. 2, pp. 106–110, 2002.
- [63] F. Qian, Y. Li, S. Gradecak, H.-G. Park, Y. Dong, Y. Ding, Z. L. Wang, and C. M. Lieber, "Multi-quantum-well nanowire heterostructures for wavelength-controlled lasers," *Nature materials*, vol. 7, no. 9, pp. 701–706, 2008.
- [64] A. Das, J. Heo, M. Jankowski, W. Guo, L. Zhang, H. Deng, and P. Bhattacharya, "Room temperature ultralow threshold GaN nanowire polariton laser," *Physical Review Letters*, vol. 107, no. 6, pp. 1–5, 2011.
- [65] C.-y. Wu, C.-t. Kuo, C.-y. Wang, and C.-l. He, "Plasmonic Green Nanolaser Based on a Metal-Oxide-Semiconductor Structure," *Nano letters*, pp. 4256–4260, 2011.

- [66] S. Deshpande, J. Heo, A. Das, and P. Bhattacharya, "Electrically driven polarized single-photon emission from an InGaN quantum dot in a GaN nanowire," *Nature communications*, vol. 4, p. 1675, jan 2013.
- [67] M. J. Holmes, K. Choi, S. Kako, M. Arita, and Y. Arakawa, "Room-Temperature Triggered Single Photon Emission from a III-Nitride Site-Controlled Nanowire Quantum Dot," *Nano letters*, jan 2014.
- [68] Y. Zhang, *Characterisation of GaN using Transmission Electron Microscopy*. PhD thesis, University of Cambridge, 2008.
- [69] C. B. C. David B. Williams, *Transmission Electron Microscopy*. Springer US, 2009.
- [70] M. A. Moram, Y. Zhang, M. J. Kappers, Z. H. Barber, and C. J. Humphreys, "Dislocation reduction in gallium nitride films using scandium nitride interlayers," *Applied Physics Letters*, vol. 91, no. 15, p. 152101, 2007.
- [71] A. Howie, "Image contrast and localized signal selection techniques," *Journal of Microscopy*, 1979.
- [72] "Characteristic x-rays." <http://www.ammrf.org.au/myscope/analysis/eds/xraygeneration/characteristic/>.
- [73] G. Divitni, *Electron microscopy studies of photo-active TiO<sub>2</sub> nanostructures*. PhD thesis, University of Cambridge, 2012.
- [74] D. J. De Rosier and A. Klug, "Reconstruction of Three Dimensional Structures from Electron Micrographs," *Nature*, vol. 217, pp. 130–134, 1968.
- [75] P. A. Midgley and R. E. Dunin-Borkowski, "Electron tomography and holography in materials science.," *Nature materials*, vol. 8, no. 4, pp. 271–280, 2009.
- [76] G. Möbus and B. J. Inkson, "Nanoscale tomography in materials science," *Materials Today*, vol. 10, no. 12, pp. 18–25, 2007.
- [77] N. Kawase, M. Kato, H. Nishioka, and H. Jinnai, "Transmission electron microtomography without the "missing wedge" for quantitative structural analysis," *Ultramicroscopy*, vol. 107, no. 1, pp. 8–15, 2007.
- [78] J. J. Fernández, J. I. Agulleiro, A. Martínez, I. García, and F. J. Chichón, "Image processing in electron tomography," *Microscopy: Science, Technology, Applications and Education*, no. Figure 1, pp. 19–28, 2010.
- [79] P. A. Midgley and M. Weyland, "3D electron microscopy in the physical sciences: The development of Z-contrast and EFTEM tomography," *Ultramicroscopy*, vol. 96, no. 3-4, pp. 413–431, 2003.
- [80] P. Gilbert, "Iterative methods for the three-dimensional reconstruction of an object from projections," *Journal of Theoretical Biology*, vol. 36, no. 1, pp. 105–117, 1972.
- [81] P. A. Penczek, "Fundamentals of Three-Dimensional Reconstruction from Projections," pp. 1–33, 2010.

- [82] J. Frank, *Electron Tomography*. Springer New York, 2006.
- [83] R. A. Oliver, “Advances in AFM for the electrical characterization of semiconductors,” *Reports on Progress in Physics*, vol. 71, p. 076501, jul 2008.
- [84] T. Zhu, *Nanoscale Electrical Characterisation of Gallium Nitride*. PhD thesis, University of Cambridge, 2010.
- [85] B. Yacobi and D. Holt, *Cathodoluminescence Microscopy of Inorganic Solids*. Springer US, 1990.
- [86] T. Puchtler, *Development of structures and materials for InGaN/GaN cavity quantum electro-dynamics*. PhD thesis, University of Cambridge, 2014.
- [87] P. R. Edwards and R. W. Martin, “Cathodoluminescence nano-characterization of semiconductors,” *Semiconductor Science and Technology*, vol. 26, p. 064005, jun 2011.
- [88] R. W. Martin, P. R. Edwards, K. P. O’Donnell, M. D. Dawson, C.-W. Jeon, C. Liu, G. R. Rice, and I. M. Watson, “Cathodoluminescence spectral mapping of III-nitride structures,” *Physica Status Solidi (a)*, vol. 201, pp. 665–672, mar 2004.
- [89] P. Sercel, H. Zarem, J. Levens, and L. Eng, “A novel technique for the direct determination of carrier diffusion lengths in GaAs/AlGaAs heterostructures using cathodoluminescence,” *International Electron Devices Meeting*, pp. 285–288, 1989.
- [90] C. L. Paul R. Edwards, Lethy Krishnan Jagadamma, Jochen Bruckbauer and R. W. M. Philip Shields, Duncan Allsopp, Tao Wang, “High-resolution cathodoluminescence hyperspectral imaging of nitride nanostructures,” *Microscopy and Microanalysis*, pp. 1212–1219, 2012.
- [91] N. M. Haegel, *Measurement of Minority Charge Carrier Diffusion Length in Gallium Nitride Nanowires Using Electron Beam Induced Current*. PhD thesis, Naval Postgraduate School, 2009.
- [92] E. Yakimov, “Electron-beam-induced-current study of defects in GaN; experiments and simulation,” *Journal of Physics: Condensed Matter*, vol. 13069, 2002.
- [93] W. Jansen and M. Slaughter, “Elemental mapping of minerals by electron microprobe.,” *American Mineralogist*, vol. 67, no. 5-6, pp. 521–533, 1982.
- [94] M. J. Wallace, P. R. Edwards, M. J. Kappers, M. A. Hopkins, F. Oehler, S. Sivaraya, R. A. Oliver, C. J. Humphreys, D. W. E. Allsopp, and R. W. Martin, “Effect of the barrier growth mode on the luminescence and conductivity micron scale uniformity of InGaN light emitting diodes,” *Journal of Applied Physics*, vol. 117, no. 11, p. 115705, 2015.
- [95] T. Ishitani and T. Yaguchi, “Cross-sectional sample preparation by focused ion beam: a review of ion-sample interaction.,” *Microscopy research and technique*, vol. 35, no. 4, pp. 320–333, 1996.

- [96] S. Bals, W. Tirry, R. Geurts, Z. Yang, and D. Schryvers, “High-quality sample preparation by low kV FIB thinning for analytical TEM measurements.,” *Microscopy and microanalysis : the official journal of Microscopy Society of America, Microbeam Analysis Society, Microscopical Society of Canada*, vol. 13, no. 2, pp. 80–86, 2007.
- [97] L. Holzer, F. Indutnyi, P. Gasser, B. Münch, and M. Wegmann, “Three-dimensional analysis of porous  $BaTiO_3$  ceramics using FIB nanotomography,” *Journal of Microscopy*, vol. 216, no. 1, pp. 84–95, 2004.
- [98] W. Rasband, “Imagej,” 1997-2017.
- [99] M. U. P. Thévenaz, U.E. Ruttmann, “A Pyramid Approach to Subpixel Registration Based on Intensity,” *IEEE Transactions on Image Processing*, vol. 7, no. 1, pp. 27–41, 1998.
- [100] W. E. Lorensen and H. E. Cline, “Marching cubes: A high resolution 3D surface construction algorithm,” *Proceedings of the 14th annual conference on Computer graphics and interactive techniques - SIGGRAPH '87*, vol. 21, no. 4, pp. 163–169, 1987.
- [101] N. K. V. D. Laak, R. A. Oliver, M. J. Kappers, and C. J. Humphreys, “Role of gross well-width fluctuations in bright , green-emitting single InGaN/GaN quantum well structures,” *Appl. Phys. Lett.*, vol. 121911, no. 2007, pp. 1–4, 2013.
- [102] R. A. Oliver, F. C.-P. Massabuau, M. J. Kappers, W. A. Phillips, E. J. Thrush, C. C. Tartan, W. E. Blenkhorn, T. J. Badcock, P. Dawson, M. A. Hopkins, D. W. E. Allsopp, and C. J. Humphreys, “The impact of gross well width fluctuations on the efficiency of GaN-based light emitting diodes,” *Applied Physics Letters*, vol. 103, no. 14, p. 141114, 2013.
- [103] A. Polyakov, N. Smirnov, A. Usikov, A. Govorkov, and B. Pushniy, “Studies of the origin of the yellow luminescence band, the nature of nonradiative recombination and the origin of persistent photoconductivity in n-GaN films,” *Solid-State Electronics*, vol. 42, no. 11, pp. 1959–1967, 1998.
- [104] S. Chichibu, A. Abare, M. Mack, M. Minsky, T. Deguchi, D. Cohen, P. Kozodoy, S. Fleischer, S. Keller, J. Speck, J. Bowers, E. Hu, U. Mishra, L. Coldren, S. DenBaars, K. Wada, T. Sota, and S. Nakamura, “Optical properties of InGaN quantum wells,” *Materials Science and Engineering: B*, vol. 59, pp. 298–306, may 1999.
- [105] J. L. Lyons, A. Janotti, and C. G. Van De Walle, “Carbon impurities and the yellow luminescence in GaN,” *Applied Physics Letters*, vol. 97, no. 15, pp. 10–13, 2010.
- [106] R. Oliver, M. Kappers, J. Sumner, R. Datta, and C. Humphreys, “Highlighting threading dislocations in MOVPE-grown GaN using an in situ treatment with SiH<sub>4</sub> and NH<sub>3</sub>,” *Journal of Crystal Growth*, vol. 289, pp. 506–514, apr 2006.
- [107] K. Watanabe, J. R. Yang, S. Y. Huang, K. Inoke, J. T. Hsu, R. C. Tu, T. Yamazaki, N. Nakanishi, and M. Shiojiri, “Formation and structure of inverted hexagonal pyramid defects in multiple quantum wells InGaN/GaN,” *Applied Physics Letters*, vol. 82, no. 5, pp. 718–720, 2003.

- [108] M. Shiojiri, C. C. Chuo, J. T. Hsu, J. R. Yang, and H. Saijo, “Structure and formation mechanism of V defects in multiple InGaN/GaN quantum well layers,” *Journal of Applied Physics*, vol. 99, no. 7, 2006.
- [109] M. M. Da Silva, a. R. Vaz, S. a. Moshkalev, and J. W. Swart, “Electrical Characterization of Platinum Thin Films Deposited by Focused Ion Beam,” *ECS Transactions*, vol. 9, no. 1, pp. 235–241, 2007.
- [110] F. de la Peña, T. Ostasevicius, V. T. Fauske, P. Burdet, P. Jokubauskas, M. Sarahan, D. Johnstone, M. Nord, J. Taillon, J. Caron, K. E. MacArthur, E. Prestat, A. Eljarrat, S. Mazzucco, T. Furnival, M. Walls, G. Donval, B. Martineau, A. Garmannslund, L. F. Zagonel, T. Aarholt, C. Gohlke, and Iygr, “hyperspy v1.1.1.”
- [111] G. Lorimer, “Quantitative X-ray microanalysis of thin specimens in the transmission electron microscope; a review,” *Mineralogical Magazine*, vol. 51, no. 359, pp. 49–60, 1987.
- [112] J. Piprek, *Nitride Semiconductor Devices: Principles and Simulation*. Wiley-VCH, january 20 ed., 2007.
- [113] J. Pal, G. Tse, V. Haxha, M. A. Migliorato, and S. Tomić, “Second-order piezoelectricity in wurtzite III-N semiconductors,” *Physical Review B - Condensed Matter and Materials Physics*, vol. 84, no. 8, pp. 1–7, 2011.
- [114] J. Piprek, “Origin of InGaN/GaN light-emitting diode efficiency improvements using tunnel-junction-cascaded active regions,” *Applied Physics Letters*, vol. 104, no. 5, pp. 2–6, 2014.
- [115] Y. Li, F. Yun, X. Su, S. Liu, W. Ding, and X. Hou, “Deep hole injection assisted by large V-shape pits in InGaN/GaN multiple-quantum-wells blue light-emitting diodes,” *Journal of Applied Physics*, vol. 116, no. 12, p. 123101, 2014.
- [116] Z. Quan, L. Wang, C. Zheng, J. Liu, and F. Jiang, “Roles of V-shaped pits on the improvement of quantum efficiency in InGaN/GaN multiple quantum well light-emitting diodes,” *Journal of Applied Physics*, vol. 116, no. 18, p. 183107, 2014.
- [117] J. H. Son, J. U. Kim, Y. H. Song, B. J. Kim, C. J. Ryu, and J. L. Lee, “Design Rule of nanostructures in light-emitting diodes for complete elimination of total internal reflection,” *Advanced Materials*, vol. 24, no. 17, pp. 2259–2262, 2012.
- [118] D. I. Florescu, S. M. Ting, J. C. Ramer, D. S. Lee, V. N. Merai, A. Parkeh, D. Lu, E. A. Armour, and L. Chernyak, “Investigation of V-Defects and embedded inclusions in InGaN/GaN multiple quantum wells grown by metalorganic chemical vapor deposition on (0001) sapphire,” *Applied Physics Letters*, vol. 83, no. 1, p. 33, 2003.
- [119] R. Datta, M. Kappers, M. Vickers, J. Barnard, and C. Humphreys, “Growth and characterisation of GaN with reduced dislocation density,” *Superlattices and Microstructures*, vol. 36, pp. 393–401, oct 2004.
- [120] K. Hiramatsu, “Epitaxial lateral overgrowth techniques used in group III nitride epitaxy,” *Journal of Physics: Condensed Matter*, vol. 13, pp. 6961–6975, aug 2001.

- [121] B. Beaumont, V. Bousquet, P. Vennéguès, M. Vaille, A. Bouillé, P. Gibart, S. Dassonneville, A. Amokrane, and B. Sieber, “Two-step method for epitaxial lateral overgrowth of GaN,” *Physica Status Solidi (A) Applied Research*, vol. 176, no. 1, pp. 567–571, 1999.
- [122] H. El-Ella, F. Rol, D. Collins, M. Kappers, R. Taylor, E. Hu, and R. Oliver, “InGaN super-lattice growth for fabrication of quantum dot containing microdisks,” *Journal of Crystal Growth*, vol. 321, pp. 113–119, apr 2011.
- [123] P. Visconti, M. A. Reschchikov, K. M. Jones, D. F. Wang, R. Cingolani, H. Morkoc, R. J. Molnar, and D. J. Smith, “Highly selective photoelectrochemical etching of nitride materials for defect investigation and device fabrication,” *Journal of Vacuum Science & Technology B: Microelectronics and Nanometer Structures*, vol. 19, no. 4, p. 1328, 2001.
- [124] C. Youtsey, L. T. Romano, R. J. Molnar, and I. Adesida, “Rapid evaluation of dislocation densities in n-type GaN films using photoenhanced wet etching,” *Applied Physics Letters*, vol. 74, no. May 2015, p. 3537, 1999.
- [125] C. Youtsey, L. T. Romano, and I. Adesida, “Gallium nitride whiskers formed by selective photoenhanced wet etching of dislocations,” *Applied Physics Letters*, vol. 73, no. 6, p. 797, 1998.
- [126] M. S. Minsky, M. White, and E. L. Hu, “Room-temperature photoenhanced wet etching of GaN,” *Applied Physics Letters*, vol. 68, no. 11, pp. 1531–1533, 1996.
- [127] D. Cherns, “The structure and optoelectronic properties of dislocations in GaN The structure and optoelectronic properties of dislocations in,” *J. Phys. Condens. Matter.*, vol. 12, p. 10205, 2000.
- [128] H. A. R. El-Ella, F. Rol, M. J. Kappers, K. J. Russell, E. L. Hu, and R. A. Oliver, “Dislocation density-dependent quality factors in InGaN quantum dot containing microdisks,” *Applied Physics Letters*, vol. 98, no. 13, p. 131909, 2011.
- [129] S. K. Rhode, M. K. Horton, M. J. Kappers, S. Zhang, C. J. Humphreys, R. O. Dusane, S. L. Sahonta, and M. A. Moram, “Mg doping affects dislocation core structures in GaN,” *Physical Review Letters*, vol. 111, no. July, pp. 1–4, 2013.
- [130] M. K. Horton, S. Rhode, S.-L. Sahonta, M. J. Kappers, S. J. Haigh, T. J. Pennycook, C. J. Humphreys, R. O. Dusane, and M. A. Moram, “Segregation of In to dislocations in InGaN,” *Nano letters*, vol. 15, no. 2, pp. 923–30, 2015.
- [131] Y. Xin, E. M. James, I. Arslan, S. Sivananthan, N. D. Browning, S. J. Pennycook, F. Omnes, B. Beaumont, J.-P. Faurie, and P. Gibart, “Direct experimental observation of the local electronic structure at threading dislocations in metalorganic vapor phase epitaxy grown wurtzite GaN thin films,” *Applied Physics Letters*, vol. 76, no. 4, p. 466, 2000.
- [132] J. Elsner, R. Jones, P. K. Sitch, V. D. Porezag, M. Elstner, T. Frauenheim, M. I. Heggie, S. Oberg, and P. R. Briddon, “Theory of Threading Edge and Screw Dislocations in GaN,” *Physical Review Letters*, vol. 79, no. 19, pp. 3672–3675, 1997.

- [133] O. Ambacher, W. Rieger, P. Ansmann, H. Angerer, T. D. Moustakas, and M. Stutzmann, “Sub-bandgap absorption of gallium nitride determined by photothermal deflection spectroscopy,” *Solid State Communications*, vol. 97, no. 5, pp. 365–370, 1996.
- [134] S. Lazar, L. Weyher, J. L abd Macht, F. D. Tichelaar, and H. W. Zandbergen, “Nanopipes in GaN: photo-etching and TEM study,” *The European Physical Journal Applied Physics*, vol. 28, pp. 265–291, 2004.
- [135] N. Vartak, A. Damle-Vartak, B. Richter, O. Dirsch, U. Dahmen, S. Hammad, and J. G. Hengstler, “Cholestasis-induced adaptive remodeling of interlobular bile ducts,” *Hepatology*, vol. 63, no. 3, 2016.
- [136] D. V. S. Rao, K. Muraleedharan, and C. J. Humphreys, “TEM specimen preparation techniques,” *Microscopy: Science, Technology, Applications and Education*, no. 320, pp. 1232–1244, 2010.
- [137] W. Bergbauer, M. Strassburg, C. Kölper, N. Linder, C. Roder, J. Lähnemann, A. Trampert, S. Fündling, S. F. Li, H.-H. Wehmann, and A. Waag, “Continuous-flux MOVPE growth of position-controlled N-face GaN nanorods and embedded InGaN quantum wells,” *Nanotechnology*, vol. 21, no. 30, p. 305201, 2010.
- [138] C. Tessarek, M. Bashouti, M. Heilmann, C. Dieker, I. Knoke, E. Spiecker, and S. Christiansen, “Controlling morphology and optical properties of self-catalyzed, mask-free GaN rods and nanorods by metal-organic vapor phase epitaxy,” *Journal of Applied Physics*, vol. 114, no. 14, 2013.
- [139] S. Zhao, H. P. T. Nguyen, M. G. Kibria, and Z. Mi, “III-Nitride nanowire optoelectronics,” *Progress in Quantum Electronics*, vol. 44, pp. 14–68, 2015.
- [140] G. Liu, B. Wen, T. Xie, A. Castillo, J.-Y. Ha, N. Sullivan, R. Debnath, A. Davydov, M. Peckerar, and A. Motayed, “Top-down fabrication of horizontally-aligned gallium nitride nanowire arrays for sensor development,” *Microelectronic Engineering*, vol. 142, pp. 58 – 63, 2015.
- [141] C. B. Maliakkal, J. P. Mathew, N. Hatui, A. A. Rahman, M. M. Deshmukh, and A. Bhattacharya, “Fabrication and characterization of gan nanowire doubly clamped resonators,” *Journal of Applied Physics*, vol. 118, no. 11, 2015.
- [142] R. Debnath, J.-Y. Ha, B. Wen, D. Paramanik, A. Motayed, M. R. King, and A. V. Davydov, “Top-down fabrication of large-area gan micro- and nanopillars,” *Journal of Vacuum Science & Technology B*, vol. 32, no. 2, 2014.
- [143] S. Dhara, C. Y. Lu, C. T. Wu, C. W. Hsu, W. S. Tu, K. H. Chen, Y. L. Wang, L. C. Chen, and B. Raj, “Focused ion beam induced nanojunction and defect doping as a building block for nanoscale electronics in GaN nanowires,” *Journal of Physical Chemistry C*, vol. 114, no. 36, pp. 15260–15265, 2010.
- [144] W. Shi, Y. Zheng, N. Wang, C. Lee, and S. Lee, “Microstructures of gallium nitride nanowires synthesized by oxide-assisted method,” *Chemical Physics Letters*, vol. 345, no. 56, pp. 377 – 380, 2001.

- [145] W. C. Hou, L. Y. Chen, W. C. Tang, and F. C. N. Hong, “Control of seed detachment in Au-assisted GaN nanowire growths,” *Crystal Growth and Design*, vol. 11, no. 4, pp. 990–994, 2011.
- [146] X. F. Duan and C. M. Lieber, “Laser-assisted catalytic growth of single crystal GaN nanowires,” *J Am Chem Soc*, vol. 122, no. 1, pp. 188–189, 2000.
- [147] C. Chèze, L. Geelhaar, A. Trampert, O. Brandt, and H. Riechert, “Collector phase transitions during vapor-solid-solid nucleation of GaN nanowires,” *Nano Letters*, vol. 10, no. 9, pp. 3426–3431, 2010.
- [148] J. Chen and C. Xue, “Catalytic growth of large-scale gan nanowires,” *Journal of Materials Engineering and Performance*, vol. 19, no. 7, pp. 1054–1057, 2010.
- [149] L. Geelhaar, C. Chèze, W. M. Weber, R. Averbeck, H. Riechert, T. Kehagias, P. Komnina, G. P. Dimitrakopoulos, and T. Karakostas, “Axial and radial growth of ni-induced gan nanowires,” *Applied Physics Letters*, vol. 91, no. 9, 2007.
- [150] G. Chen, T. McGuckin, C. J. Hawley, E. M. Gallo, P. Prete, I. Miccoli, N. Lovergne, and J. E. Spanier, “Subsurface imaging of coupled carrier transport in GaAs/AlGaAs core-shell nanowires,” *Nano Letters*, vol. 15, no. 1, pp. 75–79, 2015.
- [151] S. D. Hersee, X. Sun, and X. Wang, “The controlled growth of GaN nanowires,” *Nano Letters*, vol. 6, no. 8, pp. 1808–1811, 2006.
- [152] C. Tessarek, M. Heilmann, E. Butzen, A. Haab, H. Hardtdegen, C. Dieker, E. Spiecker, and S. Christiansen, “The role of Si during the growth of GaN micro- and nanorods,” *Crystal Growth and Design*, vol. 14, no. 3, pp. 1486–1492, 2014.
- [153] S. Li, S. Fuendling, X. Wang, S. Merzch, M. A. M. Al-Suleiman, J. D. Wei, H. H. Wehmann, A. Waag, W. Bergbauer, and M. Strassburg, “Polarity and its Influence on Growth Mechanism during MOVPE Growth of GaN Nanorods,” *Crystal Growth & Design*, vol. 11, pp. 1573–1577, 2011.
- [154] R. Koester, J. S. Hwang, C. Durand, D. L. S. Dang, and J. Eymery, “Self-assembled growth of catalyst-free gan wires by metal-organic vapour phase epitaxy,” *Nanotechnology*, vol. 21, no. 1, p. 015602, 2010.
- [155] A. B. Yankovich, A. V. Kvit, X. Li, F. Zhang, V. Avrutin, H. Y. Liu, N. Izumskaya, Ü. Özgür, H. Morkoç, and P. M. Voyles, “Hexagonal-based pyramid void defects in GaN and InGaN,” *Journal of Applied Physics*, vol. 111, no. 2, 2012.
- [156] Z. Fang, E. Robin, E. Rozas-Jimenez, A. Cros, F. Donatini, N. Mollard, J. Pernot, and B. Daudin, “Si Donor Incorporation in GaN Nanowires,” *Nano Letters*, vol. 15, no. 10, pp. 6794–6801, 2015.
- [157] J. Neugebauer, “Surfactants and antisurfactants on group-III-nitride surfaces,” *Physica Status Solidi C: Conferences*, vol. 0, no. 6 SPEC. ISS., pp. 1651–1667, 2003.
- [158] T. Markurt, L. Lymerakis, J. Neugebauer, P. Drechsel, P. Stauss, T. Schulz, T. Remmeli, V. Grillo, E. Rotunno, and M. Albrecht, “Blocking growth by an electrically active subsurface layer: The effect of si as an antisurfactant in the growth of GaN,” *Physical Review Letters*, vol. 110, no. 3, pp. 1–5, 2013.

- [159] M. Kappers, M. Moram, Y. Zhang, M. Vickers, Z. Barber, and C. Humphreys, “Interlayer methods for reducing the dislocation density in gallium nitride,” *Physica B: Condensed Matter*, vol. 401–402, pp. 296–301, dec 2007.
- [160] Vennégùès, B. Beaumont, S. Haffouz, M. Vaille, and P. Gibart, “Influence of in situ sapphire surface preparation and carrier gas on the growth mode of gan in movpe,” *Journal of Crystal Growth*, vol. 187, no. 2, pp. 167 – 177, 1998.
- [161] T. Böttcher, J. Dennermarck, R. Kröger, S. Figge, and D. Hommel, “The role of the growth temperature for the SiN interlayer deposition in GaN,” *Physica Status Solidi C: Conferences*, vol. 2042, no. 7, pp. 2039–2042, 2003.
- [162] C. Johnston, M. Kappers, M. Moram, J. Hollander, and C. Humphreys, “Assessment of defect reduction methods for nonpolar a-plane GaN grown on r-plane sapphire,” *Journal of Crystal Growth*, vol. 311, pp. 3295–3299, jun 2009.
- [163] S. Tanaka, S. Iwai, and Y. Aoyagi, “Self-assembling gan quantum dots on  $al_xga_{1-x}n$  surfaces using a surfactant,” *Applied Physics Letters*, vol. 69, no. 26, pp. 4096–4098, 1996.
- [164] R. A. Oliver, N. K. Van der Laak, M. J. Kappers, and C. J. Humphreys, “Insights into the growth mechanism of  $In_xGa_{1-x}N$  epitaxial nanostructures formed using a silane predose,” *Journal of Crystal Growth*, vol. 310, no. 15, pp. 3459–3465, 2008.
- [165] J. Unland, B. Onderka, A. Davydov, and R. Schmid-Fetze, “Thermodynamics and phase stability in the gan system,” *Journal of Crystal Growth*, vol. 256, pp. 33 – 51, 2003.
- [166] V. Schmidt, J. V. Wittemann, and U. Gosele, “Growth, Thermodynamics, and Electrical Properties of Silicon Nanowires.,” *Chemical Reviews*, vol. 110, no. 1, pp. 361–388, 2010.
- [167] J. Xie, Y. Fu, X. Ni, H. Morko, C. K. Inoki, T. S. Kuan, J. V. Foreman, and H. O. Everitt, “Low dislocation densities and long carrier lifetimes in gan thin films grown on a  $sin_x$  nanonetwork,” *Applied Physics Letters*, vol. 90, no. 4, 2007.
- [168] I. Halidou, Z. Benzarti, T. Boufaden, B. El Jani, S. Juillaguet, and M. Ramonda, “Influence of silane flow on MOVPE grown GaN on sapphire substrate by an in situ SiN treatment,” *Materials Science and Engineering B: Solid-State Materials for Advanced Technology*, vol. 110, no. 3, pp. 251–255, 2004.
- [169] S. E. Bennett, D. Holec, M. J. Kappers, C. J. Humphreys, and R. A. Oliver, “Imaging dislocations in gallium nitride across broad areas using atomic force microscopy.,” *The Review of scientific instruments*, vol. 81, p. 063701, jun 2010.
- [170] Q. Ji, L. Li, W. Zhang, J. Wang, P. Liu, Y. Xie, T. Yan, W. Yang, W. Chen, and X. Hu, “Dislocation Reduction and Stress Relaxation of GaN and InGaN Multiple Quantum Wells with Improved Performance via Serpentine Channel Patterned Mask,” *ACS Applied Materials and Interfaces*, vol. 8, no. 33, pp. 21480–21489, 2016.

- [171] R.-C. Tu, C.-J. Tun, C.-C. Chuo, B.-C. Lee, C.-E. Tsai, T.-C. Wang, J. Chi, C.-P. Lee, and G.-C. Chi, “Ultra-high-density ingan quantum dots grown by metalorganic chemical vapor deposition,” *Japanese Journal of Applied Physics*, vol. 43, no. 2B, p. L264, 2004.
- [172] W. Te-Chung, K. Hao-Chung, L. Tien-Chang, T. Ching-En, T. Min-Ying, H. Jung-Tsung, and Y. Jer-Ren, “Study of InGaN multiple quantum dots by metal organic chemical vapor deposition,” *Japanese Journal of Applied Physics, Part 1 (Regular Papers, Short Notes & Review Papers)*, vol. 45, no. 4B, pp. 3560–3563, 2006.
- [173] C. Tessarek, R. Roder, and T. Michalsky, “Improving the Optical Properties of Self-Catalyzed GaN Microrods toward Whispering Gallery Mode Lasing,” *ACS Photonics*, vol. 1, no. 10, pp. 990–997, 2014.